

Higgs production and decay processes via loop diagrams in various 6D Universal Extra Dimension Models at LHC

Kenji Nishiwaki^a

^a*Department of Physics, Kobe University,
1-1 Rokkodai-Cho, Nada-Ku, Kobe 657-8501, JAPAN*

E-mail: nishiwaki@stu.kobe-u.ac.jp

ABSTRACT: We calculate loop-induced Higgs production and decay processes which are relevant for the LHC in various six-dimensional Universal Extra Dimension models. More concretely, we focus on the Higgs production through gluon fusion and the Higgs decay into two photons induced by loop diagrams. They are one-loop leading processes and the contribution of Kaluza-Klein particles is considered to be significant. These processes are divergent in six dimensions. Therefore, we employ a momentum cutoff, whose size is fixed from the validity of perturbative calculation through naive dimensional analysis. In these six-dimensional Universal Extra Dimension models, the Higgs production cross section through gluon fusion is highly enhanced and the Higgs decay width into two photons is suppressed. In particular in the case of the compactification on Projective Sphere, these effects are remarkable. The deviation of the $h^{(0)} \rightarrow 2\gamma$ signal from the prediction of the Standard model is much greater than that in the case of the five-dimensional minimal UED model. We also consider threshold corrections in the two processes and these effect are noteworthy even when we take a higher cutoff and/or a heavy KK scale. Comparing our calculation to the recent LHC results which were published at the Lepton-Photon 2011 and at the December of 2011 is performed briefly.

KEYWORDS: Universal Extra Dimension model, Collider Physics

ARXIV EPRINT: [1101.0649](https://arxiv.org/abs/1101.0649) [hep-ph]

KOBE-TH-10-04

Contents

1	Introduction	1
2	Universal Extra Dimension on T^2/Z_4	3
3	Calculation of one loop Higgs production and decay processes	9
3.1	$2g \rightarrow h^{(0)}$ process	9
3.2	$h^{(0)} \rightarrow 2\gamma$ process	11
4	Universal Extra Dimension Models based on S^2	14
4.1	Gauge Theory on S^2	14
4.2	UED on S^2/Z_2	16
4.3	UED on Projective Sphere	19
5	Naive Dimensional Analysis	23
6	The deviation of the rates of Higgs production and its decay from the standard model predictions	25
6.1	Formulation of calculation	25
6.2	Results without threshold corrections	27
6.3	Results with threshold corrections	30
7	Summary	32
A	Feynman Rules containing scalar particle	37
B	Detail on threshold correction	39

1 Introduction

After a long shutdown, the LHC (Large Hadron Collider) restarted and new era of particle physics comes. Stimulated by the advent of two renowned works [1, 2], phenomenology in extra dimension has been well studied. Universal Extra Dimension (UED) is one of the interesting possibility along this direction and has been studied very well. In this model, all the fields describing particles of the Standard Model (SM) propagate in the bulk space.¹ The minimal UED (mUED) model is constructed with one extra spacial dimension of orbifold S^1/Z_2 [4]. This orbifold imposes the identification between the extra spacial coordinate y and $-y$ and there are two fixed points at $y = 0, \pi R$, where R is the radius of S^1 . Due to this identification four-dimensional (4D) chiral fermions describing the SM

¹ This possibility is first considered within string theory context [3].

fermions appear. One of the interesting points of UED model is that the constraints from the current experiments are very loose. The Kaluza-Klein (KK) mass scale M_{KK} , which is defined by the inverse of the compactification radius R , is constrained [4–13] in the mUED case. In UED model, the zero mode profile takes constant value and the overlap integral between zero modes and KK modes does not generate large deviation from the SM result. Therefore we can take the lower KK mass scale than in the other types of extra dimensional models. In addition, the existence of dark matter candidate is naturally explained by the KK parity, which is the remnant of the translational invariance along the extra spacial direction. The particle cosmology in the five-dimensional (5D) UED models has been studied strenuously [14–24]. The collider signature of the 5D UED models is similar to the one of the supersymmetric theory with neutralino dark matter [25]. The discrimination between these models is also well studied [26, 27].

And another thing, UED models with two spacial dimensions have been studied energetically. Six-dimensional (6D) UED models have remarkable theoretical properties, for example, prediction of the number of matter generations imposed by the condition of (global) anomaly cancellation [28], ensuring proton stability [29], generating electroweak symmetry breaking [30–32]. These topics drive us into considering such a class of models. In phenomenological point of view, there are also interesting aspects in 6D UED model. In 6D case, the KK mass spectrum is not equally-spaced, up to radiative corrections [33, 34]. And a 4D new scalar particle named “spinless adjoint” emerges in the model corresponding to a 6D gauge boson. These are un-eaten physical scalars associated to the 4D vector components of the 6D gauge bosons. These two points exert considerable influence on collider physics and particle cosmology [35–42]. These studies are executed on the 6D UED model based on two-torus T^2 [43–45]. It is noted that recently the UED models based on two-sphere S^2 are proposed and these models have interesting properties [46, 47]. In the S^2 -based models, the KK mass spectrum is totally different from that of the ordinary T^2 -based models and we consider that this difference would have an impact on collider and cosmological phenomenology.²

In this paper, we focus on the Higgs boson production and decay sequences through one-loop leading processes expected to occur at the LHC. In one-loop leading processes, the contribution of KK particles is considered to be significant. More concretely, we consider the Higgs production by gluon fusion and the Higgs decay to two photons. The former process is very important because it is the dominant Higgs production process at the LHC. The latter process becomes important in the case when Higgs boson mass is about from 120 GeV to 150 GeV. Actually, the ATLAS and CMS experiments at the CERN LHC have presented their latest results for the $\simeq 2 \text{ fb}^{-1}$ of data at the center of mass energy 7 TeV at the Lepton-Photon 2011, Mumbai, India, 22-27 August 2011 and the Higgs decay to two photons process plays a significant role at this range [56, 57].³ In the SM, the branching ratio of the decay into two photons is too small, but the signal of this process is very clear at the LHC experiments. Using the result of the above two processes, we can perform a crude

²In 5D case, there are also many approaches of considering the non-minimal UED models [48–55].

³ During revising this paper, both the ATLAS and CMS have published the new results, which claim that there is a peak around 125 GeV [58, 59].

estimation of the difference of the number of the decay events to two photons from the SM expectation value. By naive power counting argument, the production and the decay processes are known to be divergent logarithmically. We adopt the regularization scheme by use of KK momentum cutoff, which is determined by naive dimensional analysis. We also consider threshold corrections in the two processes and these effect are noteworthy, especially when we choose low cutoff scale in 6D UED.

As the end of the introduction, we show the organization of this paper briefly. In Section 2, we give a brief review of 6D UED model on T^2/Z_4 , which is one of the T^2 -based 6D UED model and has been studied well. In Section 3, we calculate the rate of the Higgs production process through gluon fusion and the Higgs decay process to two photons via loop diagrams in the 6D UED model on T^2/Z_4 . These results can be applied for the S^2 -based 6D UED cases with some modifications. In Section 4, we get an overview of gauge theory on S^2 and give a brief review of the two types of S^2 -based 6D UED models. In Section 5, we estimate the maximal cutoff scale, where the validity of perturbation will break down. In Section 6, we estimate the deviation of the rate of the Higgs production and decay processes and evaluate the difference of the event number from the SM results with/without threshold corrections. Section 7 is devoted to summary and discussions.

2 Universal Extra Dimension on T^2/Z_4

We give a brief review of UED model on T^2/Z_4 . A detailed construction of the minimal 5D UED based on S^1/Z_2 is studied in [4]. We consider a gauge theory on six-dimensional spacetime $M^4 \times T^2/Z_4$, which is a direct product of the four-dimensional Minkowski spacetime M^4 and two-torus T^2 with Z_4 orbifolding. We use the coordinate of six-dimensional spacetime defined by $x^M = (x^\mu, y, z)$ and the mostly-minus metric convention $\eta_{MN} = \text{diag}(1, -1, -1, -1, -1, -1)$.⁴ The representation of Clifford algebra which we adopt is

$$\Gamma^\mu = \gamma^\mu \otimes I_2 = \begin{bmatrix} \gamma^\mu & 0 \\ 0 & \gamma^\mu \end{bmatrix}, \quad \Gamma^y = \gamma^5 \otimes i\sigma_1 = \begin{bmatrix} 0 & i\gamma^5 \\ i\gamma^5 & 0 \end{bmatrix}, \quad \Gamma^z = \gamma^5 \otimes i\sigma_2 = \begin{bmatrix} 0 & \gamma^5 \\ -\gamma^5 & 0 \end{bmatrix}, \quad (2.1)$$

where γ^5 is 4D chirality operator and σ_i ($i = 1, 2, 3$) are Pauli matrices. To obtain 4D Weyl fermion from 6D Weyl fermion, we choose the type of orbifold as Z_4 , not as Z_2 in 5D case [43, 44]. Z_4 symmetry is realized as the rotation on the $y - z$ plane by an angle $\frac{\pi}{2}$ on T^2 . This means a bulk scalar field $\Phi(x; y, z)$ obeys the following relation:

$$\Phi_t(x, -z, y) = t\Phi_t(x, y, z). \quad (2.2)$$

t is Z_4 parity which takes the possible values $t = \pm 1, \pm i$ and all the fields are classified according to their parity. Following the general prescription [60], mode functions of T^2/Z_4

⁴Latin indices (M, N) run for 0, 1, 2, 3, y, z and Greek indices (μ, ν) run for 0, 1, 2, 3.

$f_t^{(m,n)}(y, z)$ are obtained as follows:⁵

$$f_t^{(m,n)}(y, z) = \begin{cases} \frac{1}{2\pi R} \frac{1}{\sqrt{1+3\delta_{m,0}\delta_{n,0}}} \left[\cos\left(\frac{my+nz}{R}\right) + \cos\left(\frac{ny-mz}{R}\right) \right] & \text{for } t = 1, \\ \frac{1}{2\pi R} \left[\cos\left(\frac{my+nz}{R}\right) - \cos\left(\frac{ny-mz}{R}\right) \right] & \text{for } t = -1, \\ \frac{1}{2\pi R} \left[\sin\left(\frac{my+nz}{R}\right) - i \sin\left(\frac{ny-mz}{R}\right) \right] & \text{for } t = i, \\ \frac{1}{2\pi R} \left[\sin\left(\frac{my+nz}{R}\right) + i \sin\left(\frac{ny-mz}{R}\right) \right] & \text{for } t = -i, \end{cases} \quad (2.3)$$

where m and n are y and z directional KK numbers, respectively and take the values $m \geq 1, n \geq 0$ or $m = n = 0$ (only for $t = 1$).⁶

And realizing cancellation of 6D gravitational and $SU(2)_L$ global anomalies requires the choice of 6D chiralities, for example, as follows [28]:

$$(\mathcal{Q}_-, \mathcal{U}_+, \mathcal{D}_+, \mathcal{L}_-, \mathcal{E}_+, \mathcal{N}_+), \quad (2.4)$$

whose zero modes form single generation of the standard model; $\mathcal{Q}_-^{(0)} = (u, d)_L$, $\mathcal{U}_+^{(0)} = u_R$, $\mathcal{D}_+^{(0)} = d_R$, $\mathcal{L}_-^{(0)} = (\nu, l)_L$, $\mathcal{E}_+^{(0)} = l_R$, $\mathcal{N}_+^{(0)} = \nu_R$. The \pm suffixes represent 6D chirality of each field and 6D chirality operator is defined as

$$\Gamma_7 = \gamma^5 \otimes \sigma_3. \quad (2.5)$$

Using 6D chiral projective operator $\Gamma_{\pm} \equiv \frac{1}{2}(1 \pm \Gamma_7)$, 6D Weyl fermions Ψ_{\pm} are described as follows;

$$\Psi_+ = \begin{pmatrix} \psi_{+R} \\ \psi_{+L} \end{pmatrix}, \quad \Psi_- = \begin{pmatrix} \psi_{-L} \\ \psi_{-R} \end{pmatrix}, \quad (2.6)$$

where $\psi_{L(R)}$ is a left(right)-handed 4D Weyl fermion. We can take the boundary condition of 6D fermion $\Psi_6 = (\psi, \Psi)^T$ (T : transpose) as in [62]:

$$\begin{aligned} \Psi_6(x, -z, y) &= (i)^{\frac{1}{2}+r} \left(\frac{1 + \Gamma^y \Gamma^z}{\sqrt{2}} \right) P \Psi_6(x, y, z) \\ \iff \begin{pmatrix} \psi \\ \Psi \end{pmatrix} (x, -z, y) &= \begin{pmatrix} i^r & 0 \\ 0 & i^{r+1} \end{pmatrix} P \begin{pmatrix} \psi \\ \Psi \end{pmatrix} (x, y, z). \end{aligned} \quad (2.7)$$

r is Z_4 twist factor which can takes the values ($r = 0, 1, 2, 3$) and P is group twist matrix for fundamental representation with the Z_4 identification ($P^4 = 1$), which we discuss soon later. When we choose the values of r as 0 or 3, zero mode sectors of Ψ_{\pm} become 4D chiral.

Next, we go on to the gauge sector. The boundary condition of this part is as in [62]:

$$A_{\mu}(x, i\omega) = P A_{\mu}(x, \omega) P^{-1}, \quad A_{\omega}(x, i\omega) = (-i) P A_{\omega}(x, \omega) P^{-1}. \quad (2.8)$$

⁵For simplicity, we drop the overall $-i$ factor for $t = \pm i$ cases.

⁶The complex factor i in $f_{t=\pm i}^{(m,n)}$ generates CP violating interactions after KK expansion in KK sector [61].

Here we define a complexified coordinate and a vector field component for clarity as

$$\omega \equiv \frac{y + iz}{\sqrt{2}}, \quad A_\omega \equiv \frac{A_y - iA_z}{\sqrt{2}}. \quad (2.9)$$

In UED model, we do not break the gauge symmetry by boundary condition. Then the matrix P is selected as $P = \mathbf{1}$. This means that none of the fields belonging to A_ω (or $A_{\bar{\omega}}$) takes zero mode, which is an would-be exotic SM particle. Finally we discuss the 6D scalar Φ . The boundary condition for this field is very simple:

$$\Phi(x, i\omega) = P\Phi(x, \omega). \quad (2.10)$$

Choosing $P = \mathbf{1}$, Φ 's zero mode remains and can be identified as the SM Higgs field. From above discussion, we can form the zero mode sector just as the SM one.

We write down the part of the 6D UED Lagrangian which is requisite for our calculation. The 6D action takes the form as follows:

$$\begin{aligned} S = \int_0^{2\pi R} dy \int_0^{2\pi R} dz \int d^4x & \left\{ -\frac{1}{2} \sum_{i=1}^3 \text{Tr} [F_{MN}^{(i)} F^{(i)MN}] \right. \\ & + (D^M H)^\dagger (D_M H) + \left[\mu^2 |H|^2 - \frac{\lambda_6^{(H)}}{4} |H|^4 \right] \\ & \left. + i\bar{\mathcal{Q}}_{3-} \Gamma^M D_M \mathcal{Q}_{3-} + i\bar{\mathcal{U}}_{3+} \Gamma^M D_M \mathcal{U}_{3+} - \left[\lambda_6^{(t)} \bar{\mathcal{Q}}_{3-} (i\sigma_2 H^*) \mathcal{U}_{3+} + \text{h.c.} \right] \right\}. \quad (2.11) \end{aligned}$$

$F_{MN}^{(i)}$ are the field strengths of gauge fields, where $F_{MN}^{(i)} = \partial_M A_N^{(i)} - \partial_N A_M^{(i)} - ig_6^{(i)} [A_M^{(i)}, A_N^{(i)}]$, and the gauge groups are those for $U(1)_Y$ ($i = 1$), $SU(2)_L$ ($i = 2$) and $SU(3)_C$ ($i = 3$) in the SM. The covariant derivatives D_M are expressed in our convention as

$$D_M = \partial_M - i \sum_{i=1}^3 g_6^{(i)} T^{(i)a} A_M^{(i)a}, \quad (2.12)$$

where $g_6^{(i)}$ are the six-dimensional gauge couplings and $T^{(i)a}$ are the group generators of each corresponding gauge group. H is the Higgs doublet, and μ , $\lambda_6^{(H)}$ and $\lambda_6^{(t)}$ are the usual Higgs mass, Higgs self coupling and Yukawa coupling of the top quark in 6D theory, respectively.⁷ \mathcal{Q}_{3-} is the quark doublet in third generation and \mathcal{U}_{3+} is the top quark singlet.

We are ready to derive the four-dimensional effective action by expanding all the 6D

⁷All the six-dimensional couplings are dimensionful. After the KK expansion, corresponding 4D couplings become dimensionless as they should be so.

fields by use of Eq. (2.3). The concrete forms of KK expansion are as follows:

$$A_\mu^{(i)}(x; y, z) = \frac{1}{2\pi R} \left\{ A_\mu^{(i)(0)}(x) + \sum_{m \geq 1, n \geq 0} A_\mu^{(i)(m,n)}(x) \left[\cos\left(\frac{my + nz}{R}\right) + \cos\left(\frac{ny - mz}{R}\right) \right] \right\}, \quad (2.13)$$

$$A_\omega^{(i)}(x; y, z) = \frac{1}{2\pi R} \left\{ \sum_{m \geq 1, n \geq 0} A_\omega^{(i)(m,n)}(x) \left[\sin\left(\frac{my + nz}{R}\right) + i \sin\left(\frac{ny - mz}{R}\right) \right] \right\}, \quad (2.14)$$

$$H(x; y, z) = \frac{1}{2\pi R} \left\{ H^{(0)}(x) + \sum_{m \geq 1, n \geq 0} H^{(m,n)}(x) \left[\cos\left(\frac{my + nz}{R}\right) + \cos\left(\frac{ny - mz}{R}\right) \right] \right\}, \quad (2.15)$$

$$Q_{3-}(x; y, z) = \frac{1}{2\pi R} \left(\begin{array}{c} Q_{3L}^{(0)}(x) + \sum_{m \geq 1, n \geq 0} Q_{3L}^{(m,n)} \left[\cos\left(\frac{my + nz}{R}\right) + \cos\left(\frac{ny - mz}{R}\right) \right] \\ \sum_{m \geq 1, n \geq 0} Q_{3R}^{(m,n)} \left[\sin\left(\frac{my + nz}{R}\right) - i \sin\left(\frac{ny - mz}{R}\right) \right] \end{array} \right), \quad (2.16)$$

$$U_{3+}(x; y, z) = \frac{1}{2\pi R} \left(\begin{array}{c} t_R^{(0)}(x) + \sum_{m \geq 1, n \geq 0} t_R^{(m,n)} \left[\cos\left(\frac{my + nz}{R}\right) + \cos\left(\frac{ny - mz}{R}\right) \right] \\ \sum_{m \geq 1, n \geq 0} t_L^{(m,n)} \left[\sin\left(\frac{my + nz}{R}\right) - i \sin\left(\frac{ny - mz}{R}\right) \right] \end{array} \right). \quad (2.17)$$

In the fermionic part, we choose all the twist factors as $r = 0$. Now we can find the SM fields $A_\mu^{(0)(i)}$, $H^{(0)}$, $Q_{3L}^{(0)}$ ($= (t_L^{(0)}, b_L^{(0)})^T$) and $t_R^{(0)}$ in the zero mode sectors. Here we focus on the 5D Higgs doublet in terms of 4D component fields:

$$H^{(0)} = \left(\begin{array}{c} \phi^{+(0)} \\ \frac{1}{\sqrt{2}}(v + h^{(0)} + i\chi^{(0)}) \end{array} \right), \quad H^{(m,n)} = \left(\begin{array}{c} \phi^{+(m,n)} \\ \frac{1}{\sqrt{2}}(h^{(m,n)} + i\chi^{(m,n)}) \end{array} \right). \quad (2.18)$$

At the zero mode part, v and $h^{(0)}$ are the ordinary four-dimensional Higgs Vacuum Expectation Value (VEV) and the usual SM physical Higgs field. $\phi^{+(0)}$ is the would-be Nambu-Goldstone boson of $W_\mu^{+(0)}$ and generate the longitudinal d.o.f. for $W_\mu^{+(0)}$ and $\chi^{(0)}$ is for $Z_\mu^{(0)}$. Subsequently, we take notice of the (4D) scalar KK excitation modes. In addition to the Higgs KK excitation modes $\{h^{(m,n)}, \phi^{+(m,n)}, \chi^{(m,n)}\}$, there are other excitation modes closely related to the (zero mode) massive gauge bosons, which are y and z components of 6D gauge fields.

Throughout this paper, we use information about W boson zero mode and its KK particles and their associative particles, which are zero and KK modes of ϕ^+ , W^{+y} and W^{+z} . In what follows, we discuss only the free Lagrangian with respect to the non-zero KK modes of W boson and their associative particles since the zero mode part is the same with the SM one.

From Eq. (2.11), we can read off the free Lagrangian part $S^W|_{\text{free}}$ as

$$\begin{aligned}
S^W|_{\text{free}} = & \int d^4x \sum_{m \geq 1, n \geq 0} \left\{ -\frac{1}{2} \left[F_{\mu\nu}^{W(m,n)} F^{W(m,n)\mu\nu} \right]_{\text{quad}} \right. \\
& + \frac{1}{2} \left[(\partial_\mu \phi^{+(m,n)}) (\partial^\mu \phi^{-(m,n)}) + (\partial_\mu W^{+(m,n)y}) (\partial^\mu W^{-(m,n)y}) + (\partial_\mu W^{+(m,n)z}) (\partial^\mu W^{-(m,n)z}) \right] \\
& + (m_W^2 + m_{(m,n)}^2) W_\mu^{+(m,n)} W^{\mu-(m,n)} - m_{(n)}^2 W^{+(m,n)y} W^{-(m,n)y} \\
& - m_{(m)}^2 W^{+(m,n)z} W^{-(m,n)z} + m_{(m)} m_{(n)} \left[W^{+(m,n)y} W^{-(m,n)z} + W^{-(m,n)y} W^{+(m,n)z} \right] \\
& - m_{(m,n)}^2 \phi^{+(m,n)} \phi^{-(m,n)} - im_W \phi^{-(m,n)} \left[m_{(m)} W^{+(m,n)y} + m_{(n)} W^{+(m,n)z} \right] \\
& + im_W \phi^{+(m,n)} \left[m_{(m)} W^{-(m,n)y} + m_{(n)} W^{-(m,n)z} \right] \\
& - m_W^2 \left[W^{+(m,n)y} W^{-(m,n)y} + W^{+(m,n)z} W^{-(m,n)z} \right] \\
& - im_W \left[(\partial^\mu \phi^{-(m,n)}) W_\mu^{+(m,n)} - (\partial^\mu \phi^{+(m,n)}) W_\mu^{-(m,n)} \right] \\
& - \left[m_{(m)} (\partial^\mu W^{+(m,n)y}) + m_{(n)} (\partial^\mu W^{+(m,n)z}) \right] W_\mu^{-(m,n)} \\
& \left. - \left[m_{(m)} (\partial^\mu W^{-(m,n)y}) + m_{(n)} (\partial^\mu W^{-(m,n)z}) \right] W_\mu^{+(m,n)} \right\}, \tag{2.19}
\end{aligned}$$

where $\left[F_{\mu\nu}^{W(m,n)} F^{W(m,n)\mu\nu} \right]_{\text{quad}} = (\partial^\mu W^{+(m,n)\nu} - \partial^\nu W^{+(m,n)\mu}) (\partial_\mu W_\nu^{-(m,n)} - \partial_\nu W_\mu^{-(m,n)})$ is the KK W-boson's kinetic term, m_W is the W-boson mass; $m_{(m)} = \frac{m}{R}$ and $m_{(m,n)}^2 = m_{(m)}^2 + m_{(n)}^2$ are describing the KK masses.

Here we adopt the following type of gauge-fixing term about W boson to eliminate cross terms in Eq. (2.19) as

$$\begin{aligned}
S_{\text{gf}}^W = & -\frac{1}{\xi} \int_0^{2\pi R} dy \int_0^{2\pi R} dz \int d^4x \left[\partial_\mu W^{+\mu} + \xi (\partial_y W^{+y} + \partial_z W^{+z} - im_W \phi^+) \right] \\
& \times \left[\partial_\mu W^{-\mu} + \xi (\partial_y W^{-y} + \partial_z W^{-z} + im_W \phi^-) \right]. \tag{2.20}
\end{aligned}$$

From Eq. (2.19), the mass of the field $W_\mu^{+(m,n)}$ is determined as $m_{W,(m,n)}^2 = m_W^2 + m_{(m,n)}^2$. Meanwhile, we have to diagonalize the scalar mass terms about $\phi^{+(m,n)}$, $W^{+(m,n)y}$ and $W^{+(m,n)z}$ to execute perturbative calculations. When we focus on this part $S_{\text{scalar-mass}}^W$ out of $S^W + S_{\text{gf}}^W$,

$$S_{\text{scalar-mass}}^W = - \int d^4x \sum_{m \geq 1, n \geq 0} \left(W^{+(m,n)y}, W^{+(m,n)z}, \phi^{+(m,n)} \right) \mathcal{M}_{(m,n)} \begin{pmatrix} W^{-(m,n)y} \\ W^{-(m,n)z} \\ \phi^{-(m,n)} \end{pmatrix}, \tag{2.21}$$

$$\mathcal{M}_{(m,n)} = \begin{bmatrix} m_W^2 + \xi m_{(m)}^2 + m_{(n)}^2 & -(1-\xi) m_{(m)} m_{(n)} & -i(1+\xi) m_W m_{(m)} \\ -(1-\xi) m_{(m)} m_{(n)} & m_W^2 + m_{(m)}^2 + \xi m_{(n)}^2 & -i(1+\xi) m_W m_{(n)} \\ +i(1+\xi) m_W m_{(m)} & +i(1+\xi) m_W m_{(n)} & \xi m_W^2 + m_{(m)}^2 + m_{(n)}^2 \end{bmatrix}. \tag{2.22}$$

By using those mass eigenstates $\{G^{+(m,n)}, a^{+(m,n)}, H^{+(m,n)}\}$, we can diagonalize the matrix $\mathcal{M}_{(m,n)}$ to the following form:

$$\begin{pmatrix} G^{\pm(m,n)} \\ a^{\pm(m,n)} \\ H^{\pm(m,n)} \end{pmatrix} = N_{(m,n)}^{\pm} \begin{pmatrix} W^{\pm(m,n)y} \\ W^{\pm(m,n)z} \\ \phi^{\pm(m,n)} \end{pmatrix}, \quad (2.23)$$

$$N_{(m,n)}^{\pm} = \frac{1}{m_{W,(m,n)} m_{(m,n)}} \begin{bmatrix} m_{(m)} m_{(m,n)} & m_{(n)} m_{(m,n)} & \mp i m_W m_{(m,n)} \\ \mp i m_W m_{(m)} & \mp i m_W m_{(n)} & m_{(m,n)}^2 \\ -m_{(n)} m_{W,(m,n)} & +m_{(m)} m_{W,(m,n)} & 0 \end{bmatrix}, \quad (2.24)$$

$$N_{(m,n)}^- \mathcal{M}_{(m,n)} (N_{(m,n)}^-)^{\dagger} = \text{diag}(\xi m_{W,(m,n)}^2, m_{W,(m,n)}^2, m_{W,(m,n)}^2). \quad (2.25)$$

This result means that $G^{+(m,n)}$ is the would-be Nambu-Goldstone boson of $W_{\mu}^{+(m,n)}$ and the others $a^{+(m,n)}, H^{+(m,n)}$ are physical 4D scalars. It is noted that $H^{+(m,n)}$ is called ‘‘spinless adjoint’’ because $H^{+(m,n)}$ is constructed only by extra spacial components of the 6D gauge boson $W_{\mu}^{+(m,n)}$. They contribute to $h^{(0)} \rightarrow 2\gamma$ Higgs decay process via loop diagrams.

Next, we derive the mass eigenstates of fermions. Just like the case mentioned above, we again consider the KK part only. The kinetic terms are diagonal, and therefore there is no need to discuss the part. The mass term of (m, n) -th KK mode fermions arising from Eq. (2.11) is

$$\begin{pmatrix} \bar{t}_R^{(m,n)} \\ \bar{Q}_{tR}^{(m,n)} \end{pmatrix} \begin{pmatrix} -m_{(m)} + i m_{(n)} & m_t \\ m_t & m_{(m)} + i m_{(n)} \end{pmatrix} \begin{pmatrix} t_L^{(m,n)} \\ Q_{tL}^{(m,n)} \end{pmatrix} + \text{h.c.}, \quad (2.26)$$

where m_t is the zero mode top quark mass and $Q_t^{(m,n)}$ is the upper component of the SU(2) doublet $Q_3^{(m,n)}$. By using the following unitary transformation including chiral rotation, we can derive the ordinary diagonalized Dirac mass term as follows:

$$\begin{pmatrix} t^{(m,n)} \\ Q_t^{(m,n)} \end{pmatrix} = \begin{pmatrix} e^{\frac{i}{2}\gamma^5\varphi(m,n)} & 0 \\ 0 & e^{-\frac{i}{2}\gamma^5\varphi(m,n)} \end{pmatrix} \begin{pmatrix} -\cos\alpha(m,n)\gamma^5 & \sin\alpha(m,n) \\ \sin\alpha(m,n)\gamma^5 & \cos\alpha(m,n) \end{pmatrix} \begin{pmatrix} t'^{(m,n)} \\ Q_t'^{(m,n)} \end{pmatrix}, \quad (2.27)$$

where $t'^{(m,n)}$ and $Q_t'^{(m,n)}$ are mass eigenstates of their corresponding fields with degenerate (m, n) -th level masses; $m_{t,(m,n)}^2 = m_t^2 + m_{(m,n)}^2$. The mixing angles $\varphi(m,n)$ and $\alpha(m,n)$ are determined as

$$\tan\varphi(m,n) = -\frac{m_{(n)}}{m_{(m)}}, \quad \cos 2\alpha(m,n) = \frac{m_{(m,n)}}{m_{t,(m,n)}}, \quad (2.28)$$

from the condition to obtain the ordinary diagonalized Dirac mass matrix. Now we are ready to calculate the rates of Higgs processes at the LHC. Some requisite interactions in this paper are discussed at the next section.

3 Calculation of one loop Higgs production and decay processes

We calculate some virtual effects of KK particle via loop diagrams in the Higgs production process through gluon (g) fusion $2g \rightarrow h^{(0)}$ and the Higgs decay process to two photon (γ) $h^{(0)} \rightarrow 2\gamma$. Those processes are 1-loop leading and it is expected that the effects of massive KK particles are significant. In addition, there is another 1-loop leading Higgs decay process to photon and Z-boson (Z) $h^{(0)} \rightarrow \gamma Z$, which we do not discuss in this paper. Before the concrete discussion about interactions, we have to understand the general structure of interactions which is needed for our study. In the scope of this paper, all external particles are SM particles, which are described by zero modes. This means the effective couplings which we use are obtained by the following type of integrals concerning mode functions $f_t^{(m,n)}$,

$$\int_0^{2\pi R} dy \int_0^{2\pi R} dz \left\{ f_{t_i}^{(0,0)} f_{t_j}^{(m,n)} f_{t_k}^{(m',n')} \right\} \text{ [3-point]}, \quad (3.1)$$

$$\int_0^{2\pi R} dy \int_0^{2\pi R} dz \left\{ f_{t_i}^{(0,0)} f_{t_i}^{(0,0)} f_{t_j}^{(m,n)} f_{t_k}^{(m',n')} \right\} \text{ [4-point]}, \quad (3.2)$$

where the Latin indices i, j, k, l indicate types of the particles. The Z_4 -parities t_l, t_i are determined as $t_l = t_i = 1$ and the condition $(t_j)^* = t_k$ is required from Z_4 invariance of the action in Eq. (2.11). Because of orthonormality of mode functions, we know that the integrals are non-vanishing only when $(m, n) = (m', n')$ and the integrals can be reduced to the ones for the zero modes alone. In other words, the value of the vertex containing KK modes, which are described by the above integrals, is exactly the same with the value of the corresponding vertex for the zero mode alone in the basis of gauge eigenstates.

We give a comment on the Higgs mass m_h and the lowest KK mass M_{KK} , which is defined as $1/R$ on the geometry of T^2 . In UED model, those two parameters are free, which means they are not determined by the theory, but there are some constraints on these parameters. From the result of LEP2 experiment, m_h is bounded from below as $m_h > 114$ GeV. And recently another bound is announced from the LHC experiments [56–59]. We discuss this point in Section 6.

We ignore the graviton contributions. In any 6D UED model, 6D Planck scale M_* is related to 4D Planck scale M_{pl} through a KK mass scale M_{KK} as follows:

$$M_*^2 \sim M_{\text{KK}} M_{\text{pl}}. \quad (3.3)$$

M_{pl} is approximately 10^{18} GeV and we are interested in the case $M_{\text{KK}} \sim \mathcal{O}(1)$ TeV. Then the magnitude of M_* is estimated easily as $\sim 10^{10}$ GeV and gravitons are still weakly coupled to other fields.

3.1 $2g \rightarrow h^{(0)}$ process

This gluon fusion process gets contribution only from the fermion triangle loops at 1-loop level. The SM contribution is calculated in Eq. [63, 64]. In UED model, the intermediate fermions are not only SM ones (zero modes) but also their KK excitations. Studies of the production process for the case of 5D minimal UED [65] and 6D S^2/Z_2 UED [66] are made.

We consider only contributions from the top quark and its KK states. The reason why we ignore other types of quarks and its KK modes is that the coupling of fermions to the Higgs is proportional to each zero mode quark mass, and thereby those effects are negligible in our analysis. In terms of the fermion mass eigenstates, the interactions of KK quarks are

$$\begin{aligned}
S_{\text{int}}^t &= \int d^4x \sum_{m \geq 1, n \geq 0} \\
&\times \left\{ \left(\bar{t}^{(m,n)}, \bar{Q}_t^{\prime(m,n)} \right) \left[\begin{pmatrix} 1 & 0 \\ 0 & 1 \end{pmatrix} g^{(3)} \gamma^\mu g_\mu \right. \right. \\
&\quad \left. \left. - \frac{m_t}{v} h^{(0)} \begin{pmatrix} \sin 2\alpha_{(m,n)} & \cos 2\alpha_{(m,n)} \gamma^5 \\ -\cos 2\alpha_{(m,n)} \gamma^5 & \sin 2\alpha_{(m,n)} \end{pmatrix} \right] \begin{pmatrix} t^{\prime(m,n)} \\ Q_t^{\prime(m,n)} \end{pmatrix} \right\}. \quad (3.4)
\end{aligned}$$

The production cross section of $2g \rightarrow h^{(0)}$ process is given as follows:

$$\sigma_{2g \rightarrow h^{(0)}} = \frac{\sqrt{2}\pi G_F}{64} \left(\frac{\alpha_s}{\pi} \right)^2 |F_{\text{gluonfusion}}|^2, \quad (3.5)$$

where G_F is the Fermi constant and α_s is the QCD coupling. $F_{\text{gluonfusion}}$ is the loop function, which consists of the SM top quark effect F_t^{SM} , the KK top quark effect F_t^{KK} and the threshold correction $F_{\text{gluonfusion}}^{\text{TC}}$. Then we can write $F_{\text{gluonfusion}} = F_t^{\text{SM}} + F_t^{\text{KK}} + F_{\text{gluonfusion}}^{\text{TC}}$ and F_t^{SM} is given in Ref. [64] in our notation as

$$F_t^{\text{SM}} = -2\lambda(m_t^2) + \lambda(m_t^2)(1 - 4\lambda(m_t^2))J(\lambda(m_t^2)), \quad (3.6)$$

where $\lambda(m^2)$ and the loop function $J(\lambda)$ are defined as

$$\lambda(m^2) = m^2/m_h^2, \quad (3.7)$$

$$\begin{aligned}
J(\lambda) &= \int_0^1 \frac{dx}{x} \ln \left[\frac{x(x-1)}{\lambda} + 1 - i\epsilon \right] \\
&= \begin{cases} -2 \left[\arcsin \frac{1}{\sqrt{4\lambda}} \right]^2 & (\text{for } \lambda \geq \frac{1}{4}), \\ \frac{1}{2} \left[\ln \frac{1 + \sqrt{1-4\lambda}}{1 - \sqrt{1-4\lambda}} - i\pi \right]^2 & (\text{for } \lambda < \frac{1}{4}), \end{cases} \quad (3.8)
\end{aligned}$$

respectively.⁸ The KK top quark coupling to the gluon and the zero mode Higgs is shown in Eq. (3.4). After some calculation, we can get the form of F_t^{KK} in 6D UED model, where the concrete form is

$$\begin{aligned}
F_t^{\text{KK}} &= 2 \sum_{m \geq 1, n \geq 0} \left(\frac{m_t}{m_{t,(m,n)}} \right)^2 \\
&\times \left\{ -2\lambda(m_{t,(m,n)}^2) + \lambda(m_{t,(m,n)}^2)(1 - 4\lambda(m_{t,(m,n)}^2))J(\lambda(m_{t,(m,n)}^2)) \right\}. \quad (3.9)
\end{aligned}$$

⁸Our loop function J is related to the three-point scalar Passarino-Veltman function C_0 in Refs. [67, 68] as $J = m_h^2 C_0$.

It is noted that F_t^{SM} and F_t^{KK} contain the (-1) factor due to fermionic loop. Our result is directly related to the minimal 5D case in Ref. [65]. The reason is that the only difference between 5D and 6D case is the KK top quark mass spectrum and the structure of the Feynman diagrams itself describing this process is completely the same. The m^2 in $\lambda(=m^2/m_h^2)$ indicates the intermediate mass scale propagating in the loops and we consider the situation that KK scale $m_{(m,n)}$ is much greater than the Higgs scale m_h . It is noted that we only focus on the light Higgs possibility; $120 \text{ GeV} \lesssim m_h \lesssim 150 \text{ GeV}$ and thereby we have to only consider the $\lambda \geq 1/4$ case. Finally the contribution from threshold correction is obtained as

$$F_{\text{gluonfusion}}^{\text{TC}} = \left[\left(\frac{\alpha_s}{\pi} \right) \frac{1}{v} \right]^{-1} C'_{hgg}, \quad (3.10)$$

where C'_{hgg} is a dimensionful coefficient describing the threshold correction and is related to the dimensionless constant in a part of the Lagrangian C_{hgg} with the UED cutoff scale Λ_{UED} as

$$C'_{hgg} = \frac{C_{hgg} \left(\frac{v}{\sqrt{2}} \right)}{\Lambda_{\text{UED}}^2}. \quad (3.11)$$

We see the details in Appendix B.

From naive power counting, this result is logarithmically divergent. The reason is the following. Higgs decay through gluon fusion is described with dimension-six operator in four-dimensional picture after KK reduction. In UED model, there is no shift symmetry alleviating divergence, then this process obeys the above simple estimation.⁹ Therefore, we introduce a cutoff scale Λ_{UED} to regularize the F_t^{KK} in Eq. (3.9). We estimate an upper bound of Λ_{UED} by use of Naive Dimensional Analysis (NDA) technique [4] in Section 5.

3.2 $h^{(0)} \rightarrow 2\gamma$ process

Now we turn to the Higgs decay process $h^{(0)} \rightarrow 2\gamma$, which is the experimentally favorable at the LHC with Higgs mass region $120 \text{ GeV} \lesssim m_h \lesssim 150 \text{ GeV}$. The Feynman diagrams describing $h^{(0)} \rightarrow 2\gamma$ process due to the contribution of W boson and its associated particles are shown in Fig. 1, 2, 3, and 4. $\omega_W^{(m,n)}$ and $\bar{\omega}_W^{(m,n)}$ indicate (m, n) -th ghost and anti-ghost modes originated from $W_\mu^{(m,n)}$ boson, respectively. We also need to consider a flipped ($\mu \leftrightarrow \nu$) one for each diagram if it exists. It is noted that there are another triangle loop diagrams contributing to this process, whose intermediate particles are the top quark and its KK states. But we can take these effects into account by use of the previous result in Eq. (3.9) with some modifications. The decay width can be written as

$$\Gamma_{h^{(0)} \rightarrow 2\gamma} = \frac{\sqrt{2}G_F}{16\pi} \left(\frac{\alpha_{\text{EM}}}{\pi} \right)^2 m_h^3 |F_{\text{decay}}|^2, \quad (3.12)$$

where α_{EM} is the electromagnetic coupling strength. In this process, the function describing loop effects F_{decay} is written by

$$F_{\text{decay}} = F_W + 3Q_t^2 (F_t^{\text{SM}} + F_t^{\text{KK}}) + F_{\text{decay}}^{\text{TC}}, \quad (3.13)$$

⁹In 5D UED, we can calculate this process without cutoff dependence.

where the first term represents the effect of W boson and its associated particles, and the second term represents that of the top quark and its KK states.¹⁰ The third term describes the threshold correction. The SM result for F_t^{SM} is previously obtained in Eq. (3.6) and the concrete form of F_W^{SM} is derived in [69] as

$$F_W^{\text{SM}} = \frac{1}{2} + 3\lambda(m_W^2) - 3\lambda(m_W^2)(1 - 2\lambda(m_W^2))J(\lambda(m_W^2)), \quad (3.14)$$

where J is given in Eq. (3.8). We set $F_W = F_W^{\text{SM}} + F_W^{\text{KK}}$, where F_t^{KK} has been already discussed and F_W^{KK} represents the contribution of KK W boson and its associated KK particles. And we decompose F_W^{KK} into four pieces as

$$F_W^{\text{KK}} = F_{\text{gauge}}^{\text{KK}} + F_{\text{NG}}^{\text{KK}} + F_{\text{scalar1}}^{\text{KK}} + F_{\text{scalar2}}^{\text{KK}}, \quad (3.15)$$

where each term F_W^{KK} indicates the loop effects coming from gauge, would-be NG boson, scalar particles, respectively and corresponding Feynman diagrams are found in Fig. 1, 2, 3, and 4, respectively. The four sets of diagrams are $U(1)_{EM}$ gauge invariant and we can check this fact by use of Ward identity.

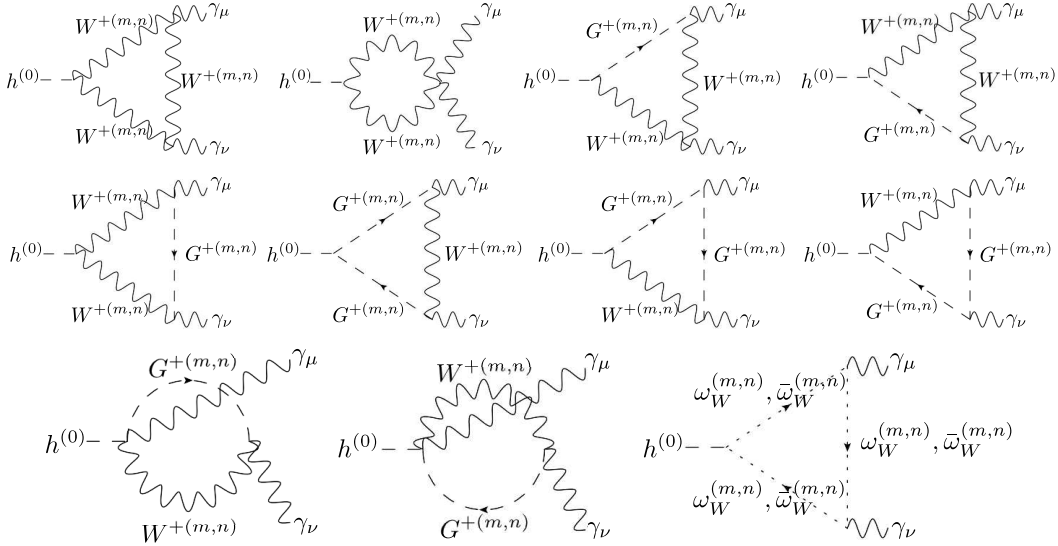


Figure 1. Feynman diagrams of 4D gauge sector describing $h^{(0)} \rightarrow 2\gamma$ process.

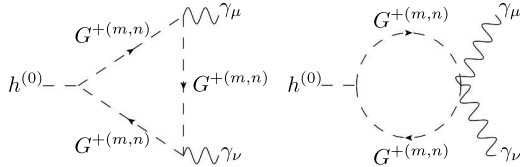


Figure 2. Feynman diagrams of 4D would-be NG boson sector describing $h^{(0)} \rightarrow 2\gamma$ process.

¹⁰3 is color factor and Q_t is the electromagnetic charge of the top quark ($= \frac{2}{3}$).

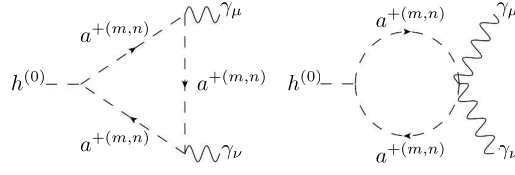


Figure 3. Feynman diagrams of 4D scalar sector describing $h^{(0)} \rightarrow 2\gamma$ process.

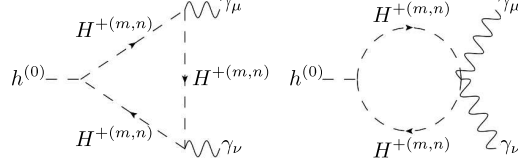


Figure 4. Feynman diagrams of 4D scalar (“spinless adjoint”) sector describing $h^{(0)} \rightarrow 2\gamma$ process.

After some tedious but straightforward calculation, we can get the result as follows:¹¹

$$F_{\text{gauge}}^{\text{KK}} = \sum_{m \geq 1, n \geq 0} \left\{ 3\lambda(m_W^2) + 2\lambda(m_W^2) (3\lambda(m_{W,(m,n)}^2) - 2) J \left(\lambda(m_{W,(m,n)}^2) \right) \right\}, \quad (3.16)$$

$$F_{\text{NG}}^{\text{KK}} = \sum_{m \geq 1, n \geq 0} \left(\frac{1}{2} \frac{m_h^2}{m_{W,(m,n)}^2} \right) \lambda(m_W^2) \left\{ 1 + 2\lambda(m_{W,(m,n)}^2) J \left(\lambda(m_{W,(m,n)}^2) \right) \right\}, \quad (3.17)$$

$$F_{\text{scalar1}}^{\text{KK}} = \sum_{m \geq 1, n \geq 0} \left(\frac{1}{2} \frac{1}{m_{W,(m,n)}^2} \right) \left[\frac{m_h^2}{m_W^2} m_{(m,n)}^2 + 2m_{W,(m,n)}^2 \right] \times \lambda(m_W^2) \left\{ 1 + 2\lambda(m_{W,(m,n)}^2) J \left(\lambda(m_{W,(m,n)}^2) \right) \right\}, \quad (3.18)$$

$$F_{\text{scalar2}}^{\text{KK}} = \sum_{m \geq 1, n \geq 0} \lambda(m_W^2) \left\{ 1 + 2\lambda(m_{W,(m,n)}^2) J \left(\lambda(m_{W,(m,n)}^2) \right) \right\}, \quad (3.19)$$

By adding up Eqs. (3.16)-(3.19), the concrete form of F_W^{KK} is given as

$$F_W^{\text{KK}} = \sum_{m \geq 1, n \geq 0} \left\{ \frac{1}{2} + 5\lambda(m_W^2) - \left[\lambda(m_W^2) (4 - 10\lambda(m_{W,(m,n)}^2)) - \lambda(m_{W,(m,n)}^2) \right] J \left(\lambda(m_{W,(m,n)}^2) \right) \right\}, \quad (3.20)$$

where we use the relation $m_{W,(m,n)}^2 = m_W^2 + m_{(m,n)}^2$. This loop-induced process is also described by dimension-six operator in 4D point of view and we have to introduce the cutoff scale Λ_{UED} to regularize the summations. The concrete form of the third term in Eq. (3.13), which originates from threshold correction, is as follows:

$$F_{\text{decay}}^{\text{TC}} = \left[\left(\frac{\alpha_{\text{EM}}}{\pi} \right) \frac{2}{v} \right]^{-1} C'_{h\gamma\gamma}, \quad (3.21)$$

¹¹In Appendix A, we write down some Feynman rules to calculate this process.

where $C'_{h\gamma\gamma}$ is a dimensionful coefficient describing the threshold correction and is related to the dimensionless constant in a part of the Lagrangian $C_{h\gamma\gamma}$ with the UED cutoff scale Λ_{UED} as

$$C'_{h\gamma\gamma} = \frac{C_{h\gamma\gamma} \left(\frac{v}{\sqrt{2}} \right)}{\Lambda_{\text{UED}}^2}. \quad (3.22)$$

We also see the details in Appendix B.

4 Universal Extra Dimension Models based on S^2

Recently, Universal Extra Dimension Models based on S^2 are proposed in Refs. [46, 47]. After an overview of gauge theory on S^2 , we give a brief review of these models.

4.1 Gauge Theory on S^2

We consider a gauge theory on six-dimensional spacetime $M^4 \times S^2$, which is a direct product of the four-dimensional Minkowski spacetime M^4 and two-sphere S^2 . We use the coordinate of six-dimensional spacetime defined by $x^M = (x^\mu, \theta, \phi)$. θ (ϕ) is zenith (azimuthal) angle of S^2 , respectively and we use the same coordinate conventions as in Section 2. The metric ansatz of $M^4 \times S^2$ is

$$g_{MN} = \text{diag}(1, -1, -1, -1, -R^2, -R^2 \sin^2 \theta) \quad (4.1)$$

and we also need to introduce the vielbein $e_M^N = \text{diag}(1, 1, 1, 1, R, R \sin \theta)$ to describe tangent space which fermions live in. In this tangent space, the coordinate is expressed with barred letters and we choose the same representation of Clifford algebra as in Eq. (2.1). S^2 has a positive curvature and then a radius of S^2 described by R only can take an infinite value by the consistency with the 6D Einstein equation. To stabilize the system, we introduce a $U(1)_X$ gauge field which has a monopole-like configuration in classical level X_M^c [70]. This configuration is defined as follows:

$$[X_\phi^c(x^\mu, \theta, \phi)]_S^N = \frac{n}{2g_6^{(X)}} (\cos \theta \mp 1), \quad (\text{other components}) = 0, \quad (4.2)$$

where $g_6^{(X)}$ is a $U(1)_X$ gauge coupling and n is a monopole index. The superscript $\frac{N}{S}$ indicates that the field is given in north (involving the $\theta = 0$ point) and south (involving the $\theta = \pi$ point) patches, respectively and we use this notation throughout the rest of this paper. The gauge transformation from the north to the south patch is given by

$$[X_M(x^\mu, \theta, \phi)]^S = [X_M(x^\mu, \theta, \phi)]^N + \frac{1}{g_6^{(X)}} \partial_M \alpha(x^\mu, \theta, \phi), \quad (4.3)$$

where the function $\alpha(x^\mu, \theta, \phi) = n\phi$. Because of the monopole-like configuration, the radius of S^2 is stabilized spontaneously as

$$R^2 = \left(\frac{n}{2g_6^{(X)} M_*^2} \right)^2. \quad (4.4)$$

Every 6D field Φ on S^2 is KK expanded by use of the spin-weighted spherical harmonics ${}_s Y_{jm}(\theta, \phi)$ as follows:¹²

$$\Phi(x, \theta, \phi)^N = \sum_{j=|s|}^{\infty} \sum_{m=-j}^j \varphi^{(j,m)}(x) f_{\Phi}^{(j,m)}(\theta, \phi)^N, \quad f_{\Phi}^{(j,m)}(\theta, \phi)^N := \frac{{}_s Y_{jm}(\theta, \phi) e^{\pm i s \phi}}{R}, \quad (4.5)$$

where s is the spin weight of the field Φ . The spin-weighted spherical harmonics ${}_s Y_{jm}(\theta, \phi)$ matches the orthonormal condition as

$$\int_0^{2\pi} d\phi \int_{-1}^1 d \cos \theta \overline{{}_s Y_{jm}(\theta, \phi)} {}_s Y_{j'm'}(\theta, \phi) = \delta_{jj'} \delta_{mm'}. \quad (4.6)$$

A spin weight of a fermion is closely related to its $U(1)_X$ charge. When we assign $U(1)_X$ charges of 6D Weyl fermions Ψ_{\pm} as $q_{\Psi_{\pm}}$, the corresponding spin weights of 4D Weyl fermions $\{\psi_{+L}^R, \psi_{-L}^R\}$ are given as follows in our convention:

$$s_{+L}^R = - \left(\frac{nq_{\Psi_+} \mp 1}{2} \right), \quad s_{-L}^R = - \left(\frac{nq_{\Psi_-} \pm 1}{2} \right). \quad (4.7)$$

We can find the fact that if a 6D Weyl fermion takes the $s = 0$ spin weight, one zero mode ($j = 0$) appears as a 4D Weyl fermion with no KK mass. This means we can get the SM fermions without orbifolding in the case of S^2 . When we take the values as $(s_{+R}, s_{+L}, s_{-R}, s_{-L}) = (0, -1, -1, 0)$, we can create the same situation as in T^2/Z_4 which we discussed before. A spin weight of a 4D vector component of a 6D gauge boson is $s = 0$ and then there is a zero mode which we can assign as a SM gauge boson. However, extra dimensional components of 6D gauge boson are expanded by the $|s| = 1$ spin-weighted spherical harmonics. This is because these parts are closely related to S^2 structure. Concretely speaking, the combinations of components $A_{\pm} = \frac{1}{\sqrt{2}}(A_{\theta} \pm iA_{\phi})$ are KK expanded with $s = \pm 1$ spin weighted spherical harmonics, respectively, where \underline{A}_M is a gauge field on tangent space defined as $\underline{A}_M = e_M^N A_N$. Then there is no zero mode in these parts. After the introduction of gauge fixing term concerning a gauge field A_M , whose concrete form is

$$- \frac{1}{\xi} \text{tr} \left(\eta^{\mu\nu} \partial_{\mu} A_{\nu} - \frac{\xi}{R^2 \sin \theta} \partial_{\theta} \sin \theta A_{\theta} - \frac{\xi}{R^2 \sin^2 \theta} A_{\phi} \right)^2 \quad (\xi : \text{gauge fixing parameter}), \quad (4.8)$$

the mass eigenstates are obtained as follows:

$$\begin{pmatrix} \underline{A}_{\theta} \\ \underline{A}_{\phi} \end{pmatrix} = \begin{pmatrix} \partial_{\theta} - \csc \theta \partial_{\phi} \\ \partial_{\theta} + \csc \theta \partial_{\phi} \end{pmatrix} \begin{pmatrix} \phi_1^{(A)} \\ \phi_2^{(A)} \end{pmatrix}. \quad (4.9)$$

$\phi_1^{(A)}$ and $\phi_2^{(A)}$ are 4D physical scalar field and unphysical would-be Nambu-Goldstone mode, respectively. A 6D scalar field can take a nonzero spin weight through the interaction with the $U(1)_X$ gauge boson. But we would like to regard the zero mode of a 6D scalar field as the SM Higgs, then the value of the spin weight must be $s = 0$.

¹²Newman-Penrose edth formalism [71] is useful for description of spin weighted spherical harmonics.

In our configuration, any (j, m) -th KK mode has the KK mass,

$$m_{(j,m)}^2 = \frac{j(j+1)}{R^2}. \quad (4.10)$$

An important point is that the form of the above KK mass is independent of the index of m . This means there are $2j + 1$ degenerated modes for each j . It is noted that each KK mode summation over j begins from one. In contrast to the T^2 case, the value of the first KK mass is represented as $M_{\text{KK}} = \sqrt{2}/R$.

We can construct an Universal Extra Dimension model on S^2 along the direction which we have discussed. But there are two problems in this model. One is absence of KK parity. In usual UED models based on orbifold, there are fixed points of orbifold discrete symmetry and KK parity is realized as a remnant of extra spatial symmetry, which is an invariance of system in exchange of fixed points. It ensures the existence of dark matter candidate in these models. But the geometry of S^2 do not have fixed point and thereby the UED on S^2 cannot possess KK parity. The other is more serious. As we discussed before, a 4D vector component of a 6D gauge boson has zero mode in S^2 . In case of the $U(1)_X$ gauge boson, which has the monopole-like configuration, this is true. We should notice that the gauge coupling of an extra massless gauge boson is severely constrained to be $g^{(X)} \lesssim 10^{-23}$ by a torsion balance experiment [72]. $g^{(X)}$ is the 4D effective coupling of the 6D $U(1)_X$ gauge coupling $g_6^{(X)}$ and is described as $g^{(X)} = g_6^{(X)}/\sqrt{4\pi R^2}$. By use of (4.4), we can estimate the value of $g^{(X)}$ in the UED model on S^2 as

$$g^{(X)} \simeq \frac{nM_{\text{KK}}}{M_{\text{pl}}}. \quad (4.11)$$

In the viewpoint of our phenomenological motivation, M_{KK} must be $\sim \mathcal{O}(1)$ TeV. In such a situation, $g^{(X)}$ becomes $\sim 10^{-15} \cdot n$ and its value is far from the experimental bound. Since monopole charge n only can take integer value, we cannot resolve this pathology by tuning of the parameter n .

Fortunately, we can solve these problems by some modifications in the S^2 geometry. In the rest of this section, we follow some essential points of these ideas.

4.2 UED on S^2/Z_2

Following Ref. [46], we take a Z_2 orbifold on the geometry of S^2 . On this orbifold, the point (θ, ϕ) is identified with $(\pi - \theta, -\phi)$. The 6D action is as follows:

$$\begin{aligned} S = \int_0^\pi d\theta \int_0^{2\pi} d\phi \int d^4x \sqrt{-g} \left\{ -\frac{1}{2} \sum_{i=1}^3 g^{MN} g^{KL} \text{Tr} [F_{MK}^{(i)} F_{NL}^{(i)}] - \frac{1}{4} g^{MN} g^{KL} [F_{MK}^{(X)} F_{NL}^{(X)}] \right. \\ \left. + g^{MN} (D_M H)^\dagger (D_N H) + \left[\mu^2 |H|^2 - \frac{\lambda_6^{(H)}}{4} |H|^4 \right] \right. \\ \left. + i \bar{\mathcal{Q}}_{3-} \Gamma^M D_M \mathcal{Q}_{3-} + i \bar{\mathcal{U}}_{3+} \Gamma^M D_M \mathcal{U}_{3+} - \left[\lambda_6^{(t)} \bar{\mathcal{Q}}_{3-} (i\sigma_2 H^*) \mathcal{U}_{3+} + \text{h.c.} \right] \right\} \quad (4.12) \end{aligned}$$

where $\sqrt{-g} = R^2 \sin \theta$. In this model, the form of 6D action and matter content are almost the same with these of the T^2/Z_4 except the existence of the $U(1)_X$ gauge field and $F_{MN}^{(X)}$ has the classical part arising from the monopole-like configuration as

$$F_{\theta\phi} = -\frac{n}{2g_6^{(X)}} \sin \theta, \quad (\text{other components}) = 0. \quad (4.13)$$

The covariant derivative of the Higgs is given in an ordinary form as

$$D_M = \partial_M - i \sum_{i=1}^3 g_6^{(i)} T^{(i)a} A_M^{(i)a}, \quad (4.14)$$

and the covariant derivatives of fermions are obtained as follows:

$$D_M = \partial_M - i \sum_{i=1}^3 g_6^{(i)} T^{(i)a} A_M^{(i)a} - i g_6^{(X)} q_\Psi (X_M^c + X_M) + \Omega_M. \quad (4.15)$$

q_Ψ is a $U(1)_X$ charge of a fermion and X_M^c is the monopole-like classical configuration in Eq. (4.2). The other additional term Ω_M is the spin connection in S^2 , whose concrete form is

$$(\Omega_\phi)^S = \frac{i}{2} (\cos \theta \mp 1) \begin{pmatrix} 1_4 & 0 \\ 0 & -1_4 \end{pmatrix}, \quad (\text{other components}) = 0, \quad (4.16)$$

where 1_4 is a four-by-four unit matrix. We can easily construct mode functions of S^2/Z_2 $f_{s,t}^{(j,m)}(\theta, \phi)$ with spin weight s in both north and south patches following the general prescription in Ref. [60] as follows:

$$f_{s,t}^{(j,m)}(\theta, \phi)^N = \begin{cases} \frac{1}{2R} [{}_s Y_{jm}(\theta, \phi) + (-1)^{j-s} {}_s Y_{j-m}(\theta, \phi)] e^{\pm i s \phi} & \text{for } t = +1 \\ \frac{1}{2R} [{}_s Y_{jm}(\theta, \phi) - (-1)^{j-s} {}_s Y_{j-m}(\theta, \phi)] e^{\pm i s \phi} & \text{for } t = -1 \end{cases}, \quad (4.17)$$

where $t = \pm 1$ is the Z_2 parity. These mode functions have the property that $f_{s,t=\pm 1}^{(j,m)}(\pi - \theta, -\phi)^N = \pm f_{s,t=\pm 1}^{(j,m)}(\theta, \phi)^S$. To realize the Z_2 symmetry, we identify a field at (θ, ϕ) in the north patch with the same field at $(\pi - \theta, -\phi)$ in the south patch. The conditions are as follows:

$$H(x, \pi - \theta, -\phi)^N = +H(x, \theta, \phi)^S, \quad (4.18)$$

$$\{A_\mu^{(i)}, X_\mu\}(x, \pi - \theta, -\phi)^N = +\{A_\mu^{(i)}, X_\mu\}(x, \theta, \phi)^S, \quad (4.19)$$

$$\{A_{\theta,\phi}^{(i)}, X_{\theta,\phi}\}(x, \pi - \theta, -\phi)^N = -\{A_{\theta,\phi}^{(i)}, X_{\theta,\phi}\}(x, \theta, \phi)^S, \quad (4.20)$$

$$\{\mathcal{Q}_{3-}, \mathcal{U}_{3+}\}(x, \pi - \theta, -\phi)^N = +i\Gamma^y \Gamma^z \{\mathcal{Q}_{3-}, \mathcal{U}_{3+}\}(x, \theta, \phi)^S, \quad (4.21)$$

where we take the choice that all gauge twist matrices are trivial ($P = \mathbf{1}$). And we define the transformation of 6D Weyl fermion Ψ_\pm from the north to the south patch as

$$\Psi_\pm^S(x, \theta, \phi) = \exp(iq_{\Psi_\pm} \alpha + 2\phi \Sigma^y \Gamma^z) \Psi_\pm^N(x, \theta, \phi), \quad (4.22)$$

where α is the $U(1)_X$ gauge transformation function in Eq. (4.3) and $\Sigma^{\underline{y}\underline{z}}$ is the $(\underline{y}, \underline{z})$ component of the local Lorentz generator of a 6D Weyl fermion.¹³ The Higgs does not transform along the patches because the Higgs does not have spin and interaction with the $U(1)_X$ gauge field. By use of the above facts and some specific information of this model,¹⁴ we can show that the action in Eq. (4.12) is equal at both the north and the south patches. Combining this result with Eqs. (4.18)-(4.21), it is clear that the Z_2 symmetry is entailed on the action in Eq. (4.12).

The specific forms of each KK expansion are as follows:

$$\begin{aligned} \{A_\mu^{(i)}, X_\mu\}(x, \theta, \phi)^N_S &= \frac{1}{\sqrt{4\pi R}} \{A_\mu^{(i)(0)}, X_\mu^{(0)}\}(x) \\ &+ \sum_{j=1}^{\infty} \sum_{m=0}^j \{A_\mu^{(i)(j,m)}, X_\mu^{(j,m)}\}(x) \cdot (\sqrt{2}(i)^{j+m}) f_{s=0, t=+1}^{(j,m)}(\theta, \phi)^N_S, \end{aligned} \quad (4.23)$$

$$\{A_\pm^{(i)}, X_\pm\}(x, \theta, \phi)^N_S = \sum_{j=1}^{\infty} \sum_{m=0}^j \{A_\pm^{(i)(j,m)}, X_\pm^{(j,m)}\}(x) \cdot (\sqrt{2}(i)^{j+m+1}) f_{s=\pm 1, t=-1}^{(j,m)}(\theta, \phi)^N_S, \quad (4.24)$$

$$H(x, \theta, \phi)^N_S = \frac{1}{\sqrt{4\pi R}} H^{(0)}(x) + \sum_{j=1}^{\infty} \sum_{m=0}^j H^{(j,m)}(x) \cdot \sqrt{2} f_{s=0, t=+1}^{(j,m)}(\theta, \phi)^N_S, \quad (4.25)$$

$$\mathcal{Q}_{3-}(x, \theta, \phi)^N_S = \left(\begin{array}{c} \frac{1}{\sqrt{4\pi R}} Q_{3L}^{(0)}(x) + \sum_{j=1}^{\infty} \sum_{m=0}^j Q_{3L}^{(j,m)}(x) \cdot \sqrt{2} f_{s=0, t=+1}^{(j,m)}(\theta, \phi)^N_S \\ \sum_{j=1}^{\infty} \sum_{m=0}^j Q_{3R}^{(j,m)}(x) \cdot \sqrt{2} f_{s=-1, t=-1}^{(j,m)}(\theta, \phi)^N_S \end{array} \right), \quad (4.26)$$

$$\mathcal{U}_{3+}(x, \theta, \phi)^N_S = \left(\begin{array}{c} \frac{1}{\sqrt{4\pi R}} t_R^{(0)}(x) + \sum_{j=1}^{\infty} \sum_{m=0}^j t_R^{(j,m)}(x) \cdot \sqrt{2} f_{s=0, t=+1}^{(j,m)}(\theta, \phi)^N_S \\ \sum_{j=1}^{\infty} \sum_{m=0}^j t_L^{(j,m)}(x) \cdot \sqrt{2} f_{s=-1, t=-1}^{(j,m)}(\theta, \phi)^N_S \end{array} \right). \quad (4.27)$$

Here we introduce suitable normalization factor ($\sqrt{2}$) in each KK modes and some phase factors ($(i)^{j+m}, (i)^{j+m+1}$) in Eqs. (4.23,4.24) to ensure the reality of these fields. The range of the summation over m shrinks from $[-j, j]$ to $[0, j]$ after the Z_2 identification. This system has two fixed points of the Z_2 symmetry at $(\theta, \phi) = (\frac{\pi}{2}, 0), (\frac{\pi}{2}, \pi)$ and under

¹³In our notation, $\Sigma^{\underline{y}\underline{z}} = \frac{-i}{2} \begin{pmatrix} 1 & 0 \\ 0 & -1 \end{pmatrix}$.

¹⁴We can find the details in Ref. [47].

the transformation of $(\theta, \phi) \rightarrow (\theta, \phi + \pi)$, mode functions behave as

$$\begin{aligned} f_{s=0,t=+1}^{(j,m)}(\theta, \phi + \pi)_S^N &= (-1)^m f_{s=0,t=+1}^{(j,m)}(\theta, \phi)_S^N, \\ f_{s=\pm 1,t=-1}^{(j,m)}(\theta, \phi + \pi)_S^N &= -(-1)^m f_{s=\pm 1,t=-1}^{(j,m)}(\theta, \phi)_S^N. \end{aligned} \quad (4.28)$$

Thereby after the fields redefinition as

$$\{A_{\pm}^{(i)(j,m)}, X_{\pm}^{(j,m)}, Q_{3R}^{(j,m)}, t_L^{(j,m)}\} \rightarrow (-1)\{A_{\pm}^{(i)(j,m)}, X_{\pm}^{(j,m)}, Q_{3R}^{(j,m)}, t_L^{(j,m)}\}, \quad (4.29)$$

we can find that each KK field has KK parity $(-1)^m$, whose origin is considered to be a remnant of KK angular momentum conservation.

We focus on the $m = 0$ modes of each j level. When we see the concrete forms of mode functions in $m = 0$, which are

$$f_{s=0,t=+1}^{(j,m=0)}(\theta, \phi)_S^N = \frac{1}{2R}(1 + (-1)^j) \cdot {}_0Y_{j0}(\theta, \phi), \quad (4.30)$$

$$f_{s=+1,t=-1}^{(j,m=0)}(\theta, \phi)_S^N = \frac{1}{2R}(1 + (-1)^j) \cdot {}_1Y_{j0}(\theta, \phi)e^{\pm i\phi}, \quad (4.31)$$

$$f_{s=-1,t=-1}^{(j,m=0)}(\theta, \phi)_S^N = \frac{1}{2R}(1 + (-1)^j) \cdot {}_{-1}Y_{j0}(\theta, \phi)e^{\mp i\phi}, \quad (4.32)$$

we find that $m = 0$ modes appear only in the case of even j . Then the degeneracy of KK masses is

$$\begin{aligned} j + 1 &\text{ for } j = \text{even}, \\ j &\text{ for } j = \text{odd}, \end{aligned} \quad (4.33)$$

since m runs from 0 to j . These results play an essential role at the Higgs production and decay processes via loop diagrams.

After the Z_2 identification, the massless zero mode of $U(1)_X$ gauge boson survives. In this model, it is assumed that the $U(1)_X$ symmetry is anomalous and it is broken at the quantum level [73]. Therefore gauge bosons should be heavy and decoupled from the low energy physics.

4.3 UED on Projective Sphere

We can also construct a UED model based on a non-orbifolding idea in Ref. [47].¹⁵ The projective sphere (PS) is a sphere S^2 with its antipodal points identified by $(\theta, \phi) \sim (\pi - \theta, \phi + \pi)$. In the UED model based on PS , the 6D action takes a different form from

¹⁵ In [47] the terminology ‘‘real projective plane’’ is employed for the compactified space, the sphere with its antipodal points being identified.

that of ordinary 6D UED model. It is written as follows:

$$\begin{aligned}
S = \int_0^\pi d\theta \int_0^{2\pi} d\phi \int d^4x \sqrt{-g} & \left\{ -\frac{1}{2} \sum_{i=1}^3 g^{MN} g^{KL} \text{Tr} [F_{MK}^{(i)} F_{NL}^{(i)}] - \frac{1}{4} g^{MN} g^{KL} [F_{MK}^{(X)} F_{NL}^{(X)}] \right. \\
& + g^{MN} (D_M H)^\dagger (D_N H) + \left[\mu^2 |H|^2 - \frac{\lambda_6^{(H)}}{4} |H|^4 \right] \\
& + \frac{1}{2} \left[i \bar{\mathcal{Q}}_{3-} \Gamma^M D_M \mathcal{Q}_{3-} + i \bar{\mathcal{Q}}_{3+} \Gamma^M D_M \mathcal{Q}_{3+} \right] + \frac{1}{2} \left[i \bar{\mathcal{U}}_{3+} \Gamma^M D_M \mathcal{U}_{3+} + i \bar{\mathcal{U}}_{3-} \Gamma^M D_M \mathcal{U}_{3-} \right] \\
& \left. - \frac{1}{2} \left[\lambda_6^{(t)} \left(\bar{\mathcal{Q}}_{3-} (i\sigma_2 H^*) \mathcal{U}_{3+} + \bar{\mathcal{Q}}_{3+} (i\sigma_2 H^*)^T \mathcal{U}_{3-} \right) + \text{h.c.} \right] \right\}. \tag{4.34}
\end{aligned}$$

Here the “1/2” factors are introduced for a later convenience. Like the S^2/Z_2 case, $F_{MN}^{(X)}$ has the classical part. A new feature of this model is that we introduce “mirror” 6D Weyl fermions $\{\mathcal{Q}_{3+}, \mathcal{U}_{3-}\}$, which have opposite 6D chirality and opposite SM and $U(1)_X$ charges when compared with the fields $\{\mathcal{Q}_{3-}, \mathcal{U}_{3+}\}$, respectively. And the covariant derivatives in this model are given as

$$D_M = \partial_M - i \sum_{i=1}^3 g_6^{(i)} T^{(i)a} A_M^{(i)a}, \quad \text{for } H, \tag{4.35}$$

$$D_M = \partial_M - i \sum_{i=1}^3 g_6^{(i)} T^{(i)a} A_M^{(i)a} - i g_6^{(X)} q_\Psi (X_M^c + X_M) + \Omega_M, \quad \text{for } \mathcal{Q}_{3-}, \mathcal{U}_{3+}, \tag{4.36}$$

$$D_M = \partial_M - i \sum_{i=1}^3 g_6^{(i)} [-T^{(i)a}]^T A_M^{(i)a} - i g_6^{(X)} q_\Psi (X_M^c + X_M) + \Omega_M, \quad \text{for } \mathcal{Q}_{3+}, \mathcal{U}_{3-}. \tag{4.37}$$

The covariant derivative of the Higgs is the same with that in the S^2/Z_2 case, but there is a difference between fermions and these “mirror” fermions. We discuss these points shortly below.

PS is a non-orientable manifold and has no fixed point. Therefore, we cannot perform identification like the S^2/Z_2 case. We focus on the 6D P and CP transformations, which are defined as

$$[6D P] = \begin{cases} A_\mu(x, \theta, \phi) \rightarrow A_\mu(x, \pi - \theta, \phi + \pi), \\ A_\theta(x, \theta, \phi) \rightarrow -A_\theta(x, \pi - \theta, \phi + \pi), \\ A_\phi(x, \theta, \phi) \rightarrow A_\phi(x, \pi - \theta, \phi + \pi), \\ \Psi(x, \theta, \phi) \rightarrow P\Psi(x, \pi - \theta, \phi + \pi), \\ H(x, \theta, \phi) \rightarrow H(x, \pi - \theta, \phi + \pi), \end{cases} \tag{4.38}$$

$$[6D CP] = \begin{cases} A_\mu(x, \theta, \phi) \rightarrow A_\mu^C(x, \pi - \theta, \phi + \pi), \\ A_\theta(x, \theta, \phi) \rightarrow -A_\theta^C(x, \pi - \theta, \phi + \pi), \\ A_\phi(x, \theta, \phi) \rightarrow A_\phi^C(x, \pi - \theta, \phi + \pi), \\ \Psi(x, \theta, \phi) \rightarrow P\Psi^C(x, \pi - \theta, \phi + \pi), \\ H(x, \theta, \phi) \rightarrow H^*(x, \pi - \theta, \phi + \pi). \end{cases} \tag{4.39}$$

Like before, we consider Ψ is a 6D fermion and the concrete shapes of 6D C and P transformations are

$$A_M^C = -A_M^T = -A_M^*, \quad \Psi^C = \Gamma^2 \Gamma^{\underline{2}} \Psi^*, \quad P = \Gamma^{\underline{2}}. \quad (4.40)$$

It must be noted that the monopole-like configuration of the $U(1)_X$ gauge boson in Eq. (4.2) behaves under the antipodal identification as

$$\{X_\phi^c\}^N(x, \pi - \theta, \phi + \pi) = -\{X_\phi^c\}^N(x, \theta, \phi) = \{(X_\phi^c)^C\}^N(x, \theta, \phi). \quad (4.41)$$

We use a property of $U(1)$ gauge field ($X_M^T = X_M$). We can notice that the monopole-like configuration is invariant under the 6D CP transformation and transition between patches. Then we consider the identification of the $U(1)_X$ gauge field as ¹⁶

$$\begin{cases} X_\mu(x, \pi - \theta, \phi + \pi)^N &= X_\mu^C(x, \theta, \phi)^N, \\ X_\theta(x, \pi - \theta, \phi + \pi)^N &= -X_\theta^C(x, \theta, \phi)^N, \\ \{X_\phi^c, X_\phi\}^N(x, \pi - \theta, \phi + \pi) &= \{(X_\phi^c)^C, X_\phi^C\}^N(x, \theta, \phi). \end{cases} \quad (4.42)$$

These conditions ensure the monopole-like configuration after the antipodal identification and projected out the non-desirable $U(1)_X$ zero mode. It is clearly understood by the additional minus factor coming from the 6D CP transformation of gauge field in Eq. (4.40). In contrast, since we want the zero modes which describe the SM gauge bosons in UED model construction, identification of $A_M^{(i)}$ should be done by another condition. We adopt the 6D P transformation and those identifications are written as

$$\begin{cases} A_\mu^{(i)}(x, \pi - \theta, \phi + \pi)^N &= A_\mu^{(i)}(x, \theta, \phi)^N, \\ A_\theta^{(i)}(x, \pi - \theta, \phi + \pi)^N &= -A_\theta^{(i)}(x, \theta, \phi)^N, \\ A_\phi^{(i)}(x, \pi - \theta, \phi + \pi)^N &= A_\phi^{(i)}(x, \theta, \phi)^N, \end{cases} \quad (4.43)$$

where it is evident that $A_\mu^{(i)}$'s zero mode survives. We also identify the Higgs with the 6D P transformation to obtain its zero mode as

$$H(x, \pi - \theta, \phi + \pi)^N = H(x, \theta, \phi)^N. \quad (4.44)$$

Finally, we discuss the identification of 6D Weyl fermions. Since 6D Weyl fermions have $U(1)_X$ charge and interact with the $U(1)_X$ gauge boson, they should be identified by the 6D CP transformation. But if we do not consider the ‘‘mirror’’ fermions, a fundamental problem arises. The 6D P transformation of fermion changes the 6D chirality like the ordinary 4D transformation. However, the 6D C transformation of fermion does not change the 6D chirality unlike the ordinary 4D case. This means 6D chirality flips under the 6D CP transformation and we should introduce the ‘‘mirror’’ fermions with opposite 6D chirality and opposite SM and $U(1)_X$ charges to perform identification. The specific forms are as follows:

$$\{\mathcal{Q}_{3+}, \mathcal{U}_{3-}\}^N(x, \pi - \theta, \phi + \pi) = P\{\mathcal{Q}_{3-}^C, \mathcal{U}_{3+}^C\}^N(x, \theta, \phi) = \Gamma^2\{\mathcal{Q}_{3-}^*, \mathcal{U}_{3+}^*\}^N(x, \theta, \phi). \quad (4.45)$$

¹⁶We pay attention the fact that identification conditions of classical field (X_ϕ^c) and quantum field (X_ϕ) must be the same.

And we determine the forms of the covariant derivatives in Eqs. (4.36,4.37) on the criterion of invariance of the action under the 6D CP transformation in advance. Using the identification conditions in Eqs. (4.42)-(4.45), we can see that the ‘‘mirror’’ fermions vanish from the action in Eq. (4.34) after the identifications as

$$\begin{aligned}
S \longrightarrow & \int_0^\pi d\theta \int_0^{2\pi} d\phi \int d^4x \sqrt{-g} \left\{ -\frac{1}{2} \sum_{i=1}^3 g^{MN} g^{KL} \text{Tr} [F_{MK}^{(i)} F_{NL}^{(i)}] - \frac{1}{4} g^{MN} g^{KL} [F_{MK}^{(X)} F_{NL}^{(X)}] \right. \\
& + g^{MN} (D_M H)^\dagger (D_N H) + \left[\mu^2 |H|^2 - \frac{\lambda_6^{(H)}}{4} |H|^4 \right] \\
& \left. + \left[i \bar{\mathcal{Q}}_{3-} \Gamma^M D_M \mathcal{Q}_{3-} \right] + \left[i \bar{\mathcal{U}}_{3+} \Gamma^M D_M \mathcal{U}_{3+} \right] - \left[\lambda_6^{(t)} \left(\bar{\mathcal{Q}}_{3-} (i\sigma_2 H^*) \mathcal{U}_{3+} \right) + \text{h.c.} \right] \right\}, \tag{4.46}
\end{aligned}$$

and we obtain a usual type of UED model action.

Next we discuss the mass spectrum of the UED model on PS . Roughly speaking, about a half of modes are projected out. First, we focus on the $U(1)_X$ gauge boson. By use of properties of spin weighted spherical harmonics, we can conclude that its identification conditions in terms of 4D KK fields are as follows:

$$X_\mu^{(j,m)}(x) = (-1)^j (X_\mu^{(j,m)})^c(x) = (-1)^{j+1} (X_\mu^{(j,m)})(x), \tag{4.47}$$

$$X_\pm^{(j,m)}(x) = (-1)^{j+1} (X_\mp^{(j,m)})^c(x), \tag{4.48}$$

$$\phi_1^{(X)(j,m)}(x) = (-1)^{j+1} (\phi_1^{(X)(j,m)})^c(x) = (-1)^j (\phi_1^{(X)(j,m)})(x), \tag{4.49}$$

$$\phi_2^{(X)(j,m)}(x) = (-1)^j (\phi_2^{(X)(j,m)})^c(x) = (-1)^{j+1} (\phi_2^{(X)(j,m)})(x), \tag{4.50}$$

where the superscript c means 4D charge conjugation and has the property that $(X_M^{(j,m)})^c(x) = -(X_M^{(j,m)})^\text{T}$. $\phi_{1,2}^{(X)}$ are a 4D physical scalar field and an unphysical would-be Nambu-Goldstone mode of $U(1)_X$ gauge field, respectively in Eq. (4.9). In Eq. (4.47), it is clear that its unwanted zero mode is projected out correctly. In PS case, the range of the summation over m does not shrink under the identification and is still $[-j, j]$. This means that degeneracy of KK masses is $2j+1$ in this model. But from Eqs. (4.47)-(4.50), we can find that the even j modes of both $X_\mu^{(j,m)}$ and $\phi_2^{(X)(j,m)}$ and the odd j modes of $\phi_1^{(X)(j,m)}$ are projected out. The structure of these mass spectrums is one of the most characteristic feature in the UED model on PS and influences the rates of the Higgs production and decay processes via loop diagrams.

Next, we go on to the gauge bosons $A_M^{(i)}$ and the Higgs H . These field are identified by the 6D P transformation and its identification conditions in terms of 4D KK fields are as follows:

$$A_\mu^{(i)(j,m)}(x) = (-1)^j (A_\mu^{(i)(j,m)})(x), \tag{4.51}$$

$$A_\pm^{(i)(j,m)}(x) = (-1)^{j+1} (A_\mp^{(i)(j,m)})(x), \tag{4.52}$$

$$\phi_1^{(i)(j,m)}(x) = (-1)^{j+1} (\phi_1^{(i)(j,m)})(x), \tag{4.53}$$

$$\phi_2^{(i)(j,m)}(x) = (-1)^j (\phi_2^{(i)(j,m)})(x). \tag{4.54}$$

$$H^{(j,m)}(x) = (-1)^j H^{(j,m)}(x). \quad (4.55)$$

From Eqs. (4.51)-(4.55), it is obvious that the even j modes of $\phi_1^{(i)(j,m)}$ and the odd j modes of $A_\mu^{(i)(j,m)}$, $\phi_2^{(i)(j,m)}$ and $H^{(j,m)}$ are projected out. As a previous argument, the zero modes of $A_\mu^{(i)(j,m)}$ do not vanish.

Finally, 6D Weyl fermion must be discussed. It is important that the ‘‘mirror’’ fermions are completely projected out from the action in Eq. (4.46) after the antipodal identification. This is interpreted that all modes of the ‘‘mirror’’ fermions $\{\mathcal{Q}_{3+}, \mathcal{U}_{3-}\}$ are erased and no mode of $\{\mathcal{Q}_{3-}, \mathcal{U}_{3+}\}$ is projected out.

We comment on the dark matter candidate briefly. In this model, there is no KK-parity because of lack of fixed points. But alternatively, the conservation of KK angular momentum exists and it implies that the lightest KK particle is stable.

5 Naive Dimensional Analysis

In 6D UED models, since the gluon fusion Higgs production and Higgs decay to two photons processes are logarithmically divergent, we must consider upper limit of the summations of KK number in such models. We review Naive Dimensional Analysis (NDA) in these 6D models briefly. Following the concept of NDA, a loop expansion parameter ϵ in D -dimensional $SU(N)$ gauge theory at a scale μ is obtained as

$$\epsilon(\mu) = \frac{1}{2} \frac{2\pi^{D/2}}{(2\pi)^D \Gamma(D/2)} N_g g_{Di}^2(\mu) \Lambda_{\text{UED}}^{D-4}, \quad (5.1)$$

where N_g is a group index, g_{Di} is a gauge coupling in D -dimensions and Λ_{UED} is a cutoff scale. The index i is introduced to express the type of gauge interaction and the remaining part is originated from D -dimensional momentum loop integral. We should mention that $g_{Di}(\mu)$, which is the effective running coupling, has energy dependency and obeys power-of-two law scaling. When we consider a 6D theory ($D = 6$) with two compact spacial directions, an effective 4D gauge coupling g_i emerges after KK decomposition and it is described with the volume of two extra dimensions V_2 as $g_i = g_{6i}/\sqrt{V_2}$. The cutoff scale μ is the scale where the perturbation breaks down $\epsilon(\Lambda_{\text{UED}}) \sim 1$. It is obvious that the upper bound of Λ_{UED} depends on the value of V_2 , whose value is $(2\pi R)^2$ in T^2 and $4\pi R^2$ in S^2 , where R is the radius of T^2 or S^2 .

Next we would like to focus on the behavior of running of the 4D effective gauge coupling strength $\alpha_i(\Lambda_{\text{UED}})$ along the energy. We consider the following renormalization group equation:

$$\alpha_{4i}^{-1}(\mu) = \alpha_{4i}^{-1}(m_Z) - \frac{\mathbf{b}_i^{\text{SM}}}{2\pi} \ln \frac{\mu}{m_Z} + 2C \frac{\mathbf{b}_i^{\text{6D}}}{2\pi} \ln \frac{\mu}{M_{\text{KK}}} - C \frac{\mathbf{b}_i^{\text{6D}}}{2\pi} \left[\left(\frac{\mu}{M_{\text{KK}}} \right)^2 - 1 \right], \quad (5.2)$$

where C represents $\pi/2$ (1) in the case of T^2 (S^2) geometry. We note that the coefficient of the quadratic term for T^2 coincides with that in Refs. [74, 75] obtained from a different regularization scheme. The value of C differs due to the structure of the background

gauge group	SM contribution (\mathbf{b}_i^{SM})	KK contribution ($\mathbf{b}_i^{6\text{D}}$)
$SU(3)_C$	-7	-2
$SU(2)_W$	-19/6	3/2
$U(1)_Y$	41/6	27/2

Table 1. Coefficients of renormalization group equation in Eq. (5.2).

geometry.¹⁷ In Eq. (5.2), we take a scheme of approximation; masses of particles are almost degenerated in each KK level regardless of type of the fields, the effect of KK particles appears after the reference energy μ exceeds the value of M_{KK} .¹⁸ The coefficients are summarized in Table. 1.¹⁹

Considering only the quadratic term, Eq. (5.2) reads

$$\alpha_{4i}^{-1}(\Lambda_{\text{UED}}) \sim \alpha_{4i}^{-1}(m_Z) - \frac{C\mathbf{b}_i^{6\text{D}} \Lambda_{\text{UED}}^2}{2\pi M_{\text{KK}}^2}. \quad (5.3)$$

From Eq. (5.3) and $\epsilon(\Lambda_{\text{UED}}) \sim 1$, we get

$$\Lambda_{\text{UED}}^2 \sim \frac{4\pi M_{\text{KK}}^2}{C(N_g + 2\mathbf{b}_i^{6\text{D}}) \alpha_{4i}(m_Z)}, \quad (5.4)$$

In the above analysis, we take values of N_g as 3, 2 and 1 in each case of $SU(3)_C$, $SU(2)_W$ and $U(1)_Y$, respectively, and adopt some latest data announced by Particle Data Group (PDG) as

$$\begin{cases} \alpha_{U(1)_Y}(m_Z)^{-1}|_{\text{MS}} = 97.99, \\ \alpha_{SU(2)_W}(m_Z)^{-1}|_{\text{MS}} = 29.46, \\ \alpha_{SU(3)_C}(m_Z)^{-1}|_{\text{MS}} = 8.445, \\ m_Z = 91.18 [\text{GeV}]. \end{cases} \quad (5.5)$$

We do not consider ‘‘TeV-scale gauge coupling unification’’ in this paper.

In the both T^2 and S^2 cases, the most stringent bounds come from the $U(1)_Y$ cutoff scales, which restrict the effective range of the perturbation the most severely. Therefore we can conclude that the ‘‘cutoff’’ scales are as follows:

$$\Lambda_{\text{UED}} \lesssim 5.3 M_{\text{KK}}, \quad \text{for } T^2\text{-case } (V_2 = (2\pi R)^2, M_{\text{KK}} = 1/R), \quad (5.6)$$

$$\Lambda_{\text{UED}} \lesssim 6.6 M_{\text{KK}}, \quad \text{for } S^2\text{-case } (V_2 = 4\pi R^2, M_{\text{KK}} = \sqrt{2}/R). \quad (5.7)$$

We truncate the KK mode summations up to these upper bounds in each case to regularize the process. Before going on to the concrete calculation, we have to declare our choice of the UED cutoff scales. We choose three patterns in T^2 and S^2 cases separately and the concrete forms are summarized in Table 2. We also list up the value of the QCD and

¹⁷Readers who are interested in the details see Appendix in Ref. [76].

¹⁸ When we consider PS model with non-orientable manifold, there are differences in KK spectrum of gauge and Higgs fields compared to that of the other ‘‘ordinary’’ UED models as we discussed before. We ignore the effect coming from this in our analysis.

¹⁹ Note that we do not employ the GUT normalization for the $U(1)_Y$ coupling and the beta function.

	T^2 -based		S^2 -based	
	high	low	high	low
KK index	$m^2 + n^2 \leq 30$	$m^2 + n^2 \leq 10$	$j(j+1) \leq 100$	$j(j+1) \leq 30$
UV cutoff	$\Lambda_{\text{UED}} \sim 5M_{\text{KK}}$	$\Lambda_{\text{UED}} \sim 3M_{\text{KK}}$	$\Lambda_{\text{UED}} \sim 7M_{\text{KK}}$	$\Lambda_{\text{UED}} \sim 4M_{\text{KK}}$

Table 2. Two choices of high and low upper bounds for KK indices and for the corresponding UV cutoff scale.

	T^2 -based		S^2 -based	
	high	low	high	low
$\alpha_s(\Lambda_{\text{UED}})^{-1}$	20.9	12.9	24.0	13.5
$\alpha_{\text{EM}}(\Lambda_{\text{UED}})^{-1}$	33.7	93.7	10.5	89.3

Table 3. The value of the QCD and electromagnetic coupling strengths at the cutoff scales.

electromagnetic coupling strengths $\{\alpha_s, \alpha_{\text{EM}}\}$ at the cutoff scales by use of Eq. (5.3) in Table 3. It is noted that the values derived from Eq. (5.3) do not depend on the value of the KK mass scale M_{KK} up to our approximation in Eq. (5.3). The electromagnetic coupling strength is defined by using $\alpha_{SU(2)_W}$ and $\alpha_{U(1)_Y}$ as

$$\alpha_{\text{EM}}(\mu)^{-1} = \alpha_{SU(2)_W}(\mu)^{-1} + \alpha_{U(1)_Y}(\mu)^{-1}. \quad (5.8)$$

6 The deviation of the rates of Higgs production and its decay from the standard model predictions

6.1 Formulation of calculation

From the discussions which we have done, we evaluate the ratio (fractional deviation) of the Higgs production cross section through gluon fusion and the Higgs decay width into two photons to the SM ones in the three types of 6D UED models, which are denoted by $\mathcal{R}_{2g \rightarrow h^{(0)}}$ and $\mathcal{R}_{h^{(0)} \rightarrow 2\gamma}$, respectively. These ratio are represented as

$$\mathcal{R}_{2g \rightarrow h^{(0)}} \equiv \frac{\sigma(2g \rightarrow h^{(0)}; \text{UED})}{\sigma(2g \rightarrow h^{(0)}; \text{SM})} = \left(1 + \frac{F_t^{\text{KK}} + F_{\text{gluonfusion}}^{\text{TC}}}{F_t^{\text{SM}}} \right)^2, \quad (6.1)$$

$$\mathcal{R}_{h^{(0)} \rightarrow 2\gamma} \equiv \frac{\Gamma(h^{(0)} \rightarrow 2\gamma; \text{UED})}{\Gamma(h^{(0)} \rightarrow 2\gamma; \text{SM})} = \left(1 + \frac{F_W^{\text{KK}} + 3Q_t^2 F_t^{\text{KK}} + F_{\text{decay}}^{\text{TC}}}{F_W^{\text{SM}} + 3Q_t^2 F_t^{\text{SM}}} \right)^2. \quad (6.2)$$

We have obtained $F_W^{\text{KK}}, F_t^{\text{KK}}, F_{\text{gluonfusion}}^{\text{TC}}$ and $F_{\text{decay}}^{\text{TC}}$ in Section 3 in the case of T^2/Z_4 by 1-loop calculation and we can apply these results for the S^2/Z_2 and the PS cases with some modifications. It is important that the $U(1)_X$ gauge boson does not contribute to either the production process and the decay process at the 1-loop level. Therefore no new type of diagram appears and only difference appears in the KK mass spectrum and the

multiplicity of each KK mode. Once the Z_2 orbifolding or the antipodal identification is understood, the structure of KK mass spectrum itself is the same as the case of S^2 up to degeneracy. We summarize the information which is needed for the estimation in Table 4. In the S^2/Z_2 case, the KK state multiplicity is the same irrespective of the type of field.

type of field	S^2/Z_2 case	PS case
fermion	$j + 1$ for $j = \text{even}$ j for $j = \text{odd}$	$2j + 1$ for $j = \text{even}$ $2j + 1$ for $j = \text{odd}$
“mirror” fermion	N/A	0 for $j = \text{even}$ 0 for $j = \text{odd}$
gauge boson & would-be NG boson & scalar(Higgs)	$j + 1$ for $j = \text{even}$ j for $j = \text{odd}$	$2j + 1$ for $j = \text{even}$ 0 for $j = \text{odd}$
scalar(“spinless adjoint”)	$j + 1$ for $j = \text{even}$ j for $j = \text{odd}$	0 for $j = \text{even}$ $2j + 1$ for $j = \text{odd}$

Table 4. Multiplicities of fields at j level in S^2 -based UED models.

With the modification

$$\sum_{m \geq 1, n \geq 0} \rightarrow \sum_{j \geq 1} n_{S^2/Z_2}(j), \quad m_{(m,n)} \rightarrow m_{(j,m)}, \quad (6.3)$$

where $n_{S^2/Z_2}(j)$ shows the multiplicity of each level of KK modes ($j + 1$ for $j = \text{even}$ or j for $j = \text{odd}$) and $m_{(j,m)}$ is the KK mass on S^2 in Eq. (4.10), we can obtain the results as follows:

$$F_t^{\text{KK}} = 2 \sum_{j \geq 1} n_{S^2/Z_2}(j) \left(\frac{m_t}{m_{t,(j,m)}} \right)^2 \times \left\{ -2\lambda(m_{t,(j,m)}^2) + \lambda(m_{t,(j,m)}^2)(1 - 4\lambda(m_{t,(j,m)}^2))J\left(\lambda(m_{t,(j,m)}^2)\right) \right\}, \quad (6.4)$$

$$F_W^{\text{KK}} = \sum_{j \geq 1} n_{S^2/Z_2}(j) \left\{ \frac{1}{2} + 5\lambda(m_W^2) - \left[\lambda(m_W^2)(4 - 10\lambda(m_{W,(j,m)}^2)) - \lambda(m_{W,(j,m)}^2) \right] J\left(\lambda(m_{W,(j,m)}^2)\right) \right\}, \quad (6.5)$$

where we use $J(m^2)$ in Eq. (3.8). In PS case, we should pay attention to the KK state multiplicity of each type of field. There is no contribution from the “mirror” fermions. The

concrete forms are as follows:

$$F_t^{\text{KK}} = 2 \sum_{j \geq 1} (2j+1) \left(\frac{m_t}{m_{t,(j,m)}} \right)^2 \times \left\{ -2\lambda(m_{t,(j,m)}^2) + \lambda(m_{t,(j,m)}^2)(1 - 4\lambda(m_{t,(j,m)}^2))J\left(\lambda(m_{t,(j,m)}^2)\right) \right\}, \quad (6.6)$$

$$F_{\text{gauge}}^{\text{KK}} = \sum_{j \geq 1} n_{PS\text{even}}(j) \left\{ 3\lambda(m_W^2) + 2\lambda(m_W^2)(3\lambda(m_{W,(j,m)}^2) - 2)J\left(\lambda(m_{W,(j,m)}^2)\right) \right\}, \quad (6.7)$$

$$F_{\text{NG}}^{\text{KK}} = \sum_{j \geq 1} n_{PS\text{even}}(j) \left(\frac{1}{2} \frac{m_h^2}{m_{W,(j,m)}^2} \right) \lambda(m_W^2) \left\{ 1 + 2\lambda(m_{W,(j,m)}^2)J\left(\lambda(m_{W,(j,m)}^2)\right) \right\}, \quad (6.8)$$

$$F_{\text{scalar1}}^{\text{KK}} = \sum_{j \geq 1} n_{PS\text{even}}(j) \left(\frac{1}{2} \frac{1}{m_{W,(j,m)}^2} \right) \left[\frac{m_h^2}{m_W^2} m_{(j,m)}^2 + 2m_{W,(j,m)}^2 \right] \times \lambda(m_W^2) \left\{ 1 + 2\lambda(m_{W,(j,m)}^2)J\left(\lambda(m_{W,(j,m)}^2)\right) \right\}, \quad (6.9)$$

$$F_{\text{scalar2}}^{\text{KK}} = \sum_{j \geq 1} n_{PS\text{odd}}(j) \lambda(m_W^2) \left\{ 1 + 2\lambda(m_{W,(j,m)}^2)J\left(\lambda(m_{W,(j,m)}^2)\right) \right\}, \quad (6.10)$$

where $n_{PS\text{even}}(j)$: $2j+1$ for $j = \text{even}$, 0 for $j = \text{odd}$ and $n_{PS\text{odd}}(j)$: 0 for $j = \text{even}$, $2j+1$ for $j = \text{odd}$. We have already discussed the cutoff scale in both the T^2 and S^2 cases concretely in Section 5 and we are ready to estimate the ratio in the various 6D UED models.

6.2 Results without threshold corrections

The numerical results of the ratios of the production cross section via gluon fusion to the standard model prediction $\mathcal{R}_{2g \rightarrow h^{(0)}}$ are given as functions of the first KK mass scale (M_{KK}) in a unit of GeV in Fig. 5. In this paper, we consider two possibilities of Higgs mass; $m_h = 120$ GeV and $m_h = 145$ GeV and take the KK mass range between 600 GeV and 2000 GeV. We use the values of the W boson mass m_W and the top quark mass m_t , which are $m_W = 80.3$ GeV, $m_t = 173$ GeV.

From top to bottom, the green, blue, red curves represent the results of PS , S^2/Z_2 , T^2/Z_4 with $m_h = 120$ GeV, providing no threshold correction, respectively. Each black dashed line near the lines for $m_h = 120$ GeV corresponds to that with $m_h = 145$ GeV. The left, right are these with the high, low cutoff choices, respectively. It is noted that the $\mathcal{R}_{2g \rightarrow h^{(0)}} = 1$ shows the SM predictions and there are few differences between $m_h = 120$ GeV case and $m_h = 145$ GeV case in all the models. Contrast to the case of little Higgs [77–79] or gauge-Higgs unification [80–82], the contribution from KK fermions is constructive and the results of UED cases are enhanced compared to the SM prediction. These results are naturally understood because the number of the intermediate particles are much greater than these of the SM.²⁰ It is expected that 6D UED models predict a significant collider signature in the Higgs production at the LHC, especially in the PS case. The origin of the remarkable enhancement in the PS case is that numerous fermions contribute to the production process in each KK level. Besides, we can find the fact that

²⁰These results are consistent with the results in Ref. [66].

when we choose the higher cutoff, the larger number of KK top modes propagate in the triangle loop and therefore the deviation from the SM gets significant. This tendency do not depend on the type of the 6D UED models.

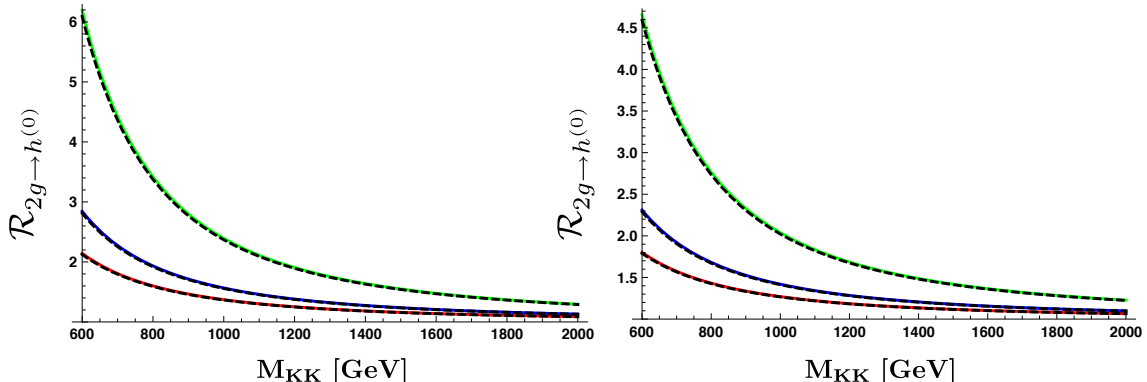


Figure 5. These plots represent the ratios of the Higgs boson production cross sections via gluon fusion to the SM prediction $\mathcal{R}_{2g \rightarrow h^{(0)}}$ in 6D UED on PS (green), S^2/Z_2 (blue), T^2/Z_4 (red) with $m_h = 120$ GeV providing no threshold correction from top to bottom. Each black dashed line near the lines for $m_h = 120$ GeV corresponds to that with $m_h = 145$ GeV. The left, right are these with the high, low cutoff choices, respectively.

The numerical results of the ratios of the rate of Higgs decay into two photons $\mathcal{R}_{h^{(0)} \rightarrow 2\gamma}$ are also given as functions of the first KK mass scale (M_{KK}) in a unit of GeV in Fig. 6. From bottom to top, the green, blue, red curves represent the results of PS , S^2/Z_2 , T^2/Z_4 with $m_h = 120$ GeV, providing no threshold correction, respectively. Each black dashed line located above the lines for $m_h = 120$ GeV corresponds to that with $m_h = 145$ GeV. The left, right are these with the high, low cutoff choices, respectively. Differently from the production, the ratios are suppressed because the contributions from quarks and gauge bosons are destructive each other. The reason of the large reduction in the PS case is understood as the results of the enormous effects of KK top quarks, which we discussed before. In any type of 6D UED models, this ratio takes the lower value than 5D mUED one. We can find some differences between $m_h = 120$ GeV and $m_h = 145$ GeV in each case of 6D UED model, which are sizable in particular at the KK mass range between 600 GeV and 1200 GeV.

We now define a value defined as

$$\Delta \equiv \mathcal{R}_{2g \rightarrow h^{(0)}} \times \mathcal{R}_{h^{(0)} \rightarrow 2\gamma}, \quad (6.11)$$

which shows the “total ratio” of the deviation of the $h^{(0)} \rightarrow 2\gamma$ signals coming from the $2g \rightarrow h^{(0)}$ Higgs production. At the LHC, the Higgs production process through gluon fusion is dominant and the value of Δ is considered to be an appropriate approximation of the $h^{(0)} \rightarrow 2\gamma$ signal deviation coming from all the Higgs production processes. Of course the numerical results of Δ are given as functions of the first KK mass scale (M_{KK}) in a unit of GeV and are shown in Fig. 7. It should be noted that in 6D UED models, the collider signal deviations from the SM in the $h^{(0)} \rightarrow 2\gamma$ process take the greater values than in

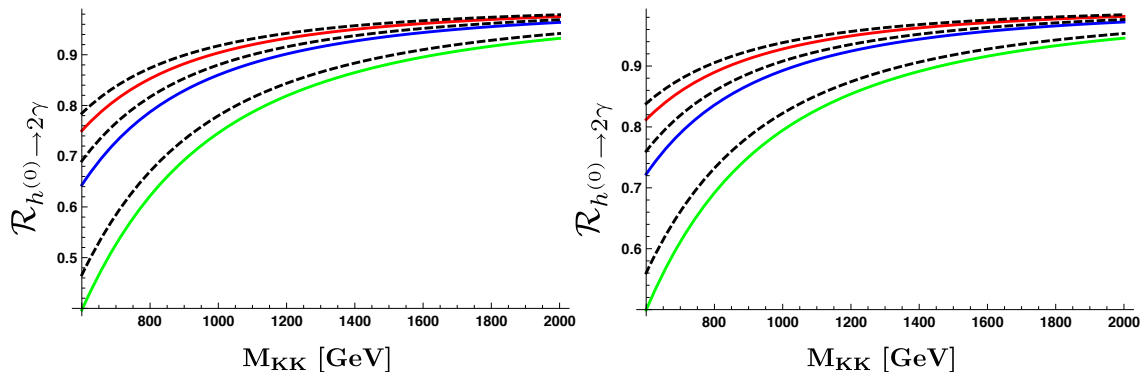


Figure 6. These plots represent the ratios of the Higgs boson decay width to two photons to the SM prediction $\mathcal{R}_{h^{(0)} \rightarrow 2\gamma}$ in 6D UED on PS (green), S^2/Z_2 (blue), T^2/Z_4 (red) with $m_h = 120$ GeV providing no threshold correction from bottom to top. Each black dashed line located above the lines for $m_h = 120$ GeV corresponds to that with $m_h = 145$ GeV. The left, right are these with the high, low cutoff choices, respectively.

the 5D mUED case. When we take the reference value as $M_{KK} = 800$ GeV in the $m_h = 120$ GeV and each high cutoff case, approximately 40%(T^2/Z_4), 60%(S^2/Z_2), 110%(PS) enhancements from the SM expectation value can be seen. It should be mentioned that the shapes of Δ in each model do not have large dependence on the value of the UED cutoff Λ_{UED} . This reason can be considered that the behavior of the ratios of the gluon fusion Higgs production and the Higgs decay to two photons is opposite when we change the value of the cutoff and a large part of the distinctions due to the value of the cutoff are cancelled out. This property is accidental but do not depend on the type of the background geometry and thereby we consider that this is one of the interesting aspects of 6D UED model. The difference between the above results and the SM expectation value is significant and we hope that this could be tested at the LHC experiments in the near future.

Finally, we comment on the up-to-date collider experimental results at the LHC. The ATLAS group announced their results, which conclude the upper limit of the cross section of the $h^{(0)} \rightarrow 2\gamma$ process in the form of the ratio to the SM result (σ/σ_{SM}) based on the 1.7 fb^{-1} data within the 95% confidence level in the August of 2011. According to [56], the value of the upper bound of (σ/σ_{SM}) is about 3.5 (5.0) at the point of $m_h = 120$ GeV ($m_h = 145$ GeV). The CMS group also announced their results, which says that the value of the upper bound of (σ/σ_{SM}) is about 3.5 (4.0) at the point of $m_h = 120$ GeV ($m_h = 145$ GeV) [57]. And at the December of 2011, the new results have been published by both the ATLAS and CMS. The ATLAS claims that there is an excess of events close to 126 GeV with a 3.6σ confidence [58]. On the other hand, the excess also have been observed by the CMS, but the location of the peak is 124 GeV with a 3.1σ confidence [59]. It is noted that both results are these before taking looking-elsewhere effect. The allowed region of the SM Higgs becomes highly constrained as $115.5 \text{ GeV} < m_h < 127 \text{ GeV}$ except the unexplored high mass region $m_h > 600$ GeV.

We do not execute detailed analysis in this paper on this topics but we can conclude

from our result in Fig. 7 that the T^2/Z_4 , S^2/Z_2 , and PS 6D UED with $m_h = 120$ GeV still survive only in the KK mass region above $M_{\text{KK}} = 600, 750, 1150$ GeV, respectively, when we consider the high cutoffs, judging from the constraint on the value of $\sigma/\sigma_{\text{SM}}$ in the December's ATLAS and CMS results, whose maximum value is roughly 1.6.²¹

It is obvious that the possibility of $m_h = 145$ GeV is discarded in all the 6D UED models since the signals are expected to be greater than these in the SM.

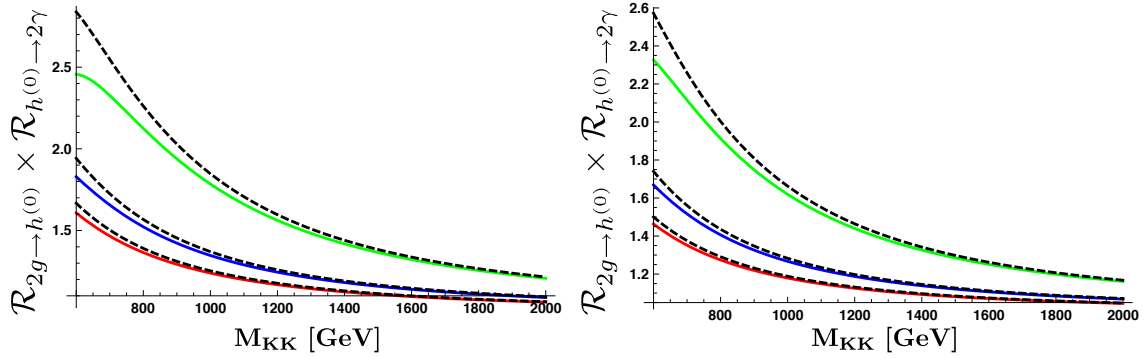


Figure 7. These plots represent the values of Δ (total ratio) in 6D UED on PS (green), S^2/Z_2 (blue), T^2/Z_4 (red) with $m_h = 120$ GeV providing each high cutoff case and no threshold correction from top to bottom. Each black dashed line located above the lines for $m_h = 120$ GeV corresponds to that with $m_h = 145$ GeV. The left, right are these with the high, low cutoff choices, respectively.

6.3 Results with threshold corrections

When we switch on the threshold corrections accompanying the processes of $2g \rightarrow h^{(0)}$ and $h^{(0)} \rightarrow 2\gamma$, the shapes of the ratios $\{\mathcal{R}_{2g \rightarrow h^{(0)}}, \mathcal{R}_{h^{(0)} \rightarrow 2\gamma}\}$ and the total ratios Δ are modified forcefully. There are two dimensionless new parameters in Eqs. (3.11,3.22) $C_{hgg}, C_{h\gamma\gamma}$, which describe the threshold correction in the process of $2g \rightarrow h^{(0)}$ or $h^{(0)} \rightarrow 2\gamma$, respectively. In this paper, we only consider some extremal choices of $C_{hgg}, C_{h\gamma\gamma}$ as

$$C_{hgg} = 0, \pm 1, \quad C_{h\gamma\gamma} = 0, \pm 1. \quad (6.12)$$

We mention that the plus/minus sign of $C_{hgg}, C_{h\gamma\gamma}$ determines the direction of interference effects to the UED part. We show the results of our numerical calculations in Figs. 8-16. We write down our convention about the color/shape of curves in Figs. 14,15,16 (total ratios) in Table 5. In the range of our approximation, the values of $\alpha_s^{-1}(m_h)$ and $\alpha_{\text{EM}}^{-1}(m_h)$ only appears in the terms describing the threshold corrections in Eqs. (3.11,3.22) and we adopt these values at the Z boson mass pole as $\alpha_s^{-1}(m_Z) = 8.44, \alpha_{\text{EM}}^{-1}(m_Z) = 127$ with ignoring the renormalization group effects between m_Z and m_h ($= 120$ or 145 GeV). We make several comments in order.

²¹ We note that the newer CMS diphoton data set includes vector boson fusion (VBF) events that occurs at the tree level in the SM. The VBF Higgs production process is not significantly enhanced by the UED loop effects.

- In the gluon fusion process in each model, due to the (-1) factor which originates from Fermi statistics in F_t^{SM} , the interference term between the threshold correction and the UED effect is destructive (constructive) in case of $C_{hgg} = +1$ (-1), respectively. It is considered that the degree of a threshold correction is inversely proportional to the value of a cutoff. When we look at the PS case with its high cutoff choice in Fig. 10, we notice that the threshold correction works a little compared to the cases of the T^2/Z_4 or S^2/Z_2 . We can find some differences between the cases of PS and S^2/Z_2 with a same cutoff value, which stem from the differences in the corresponding UED contributions. We mention that the threshold correction is still observable in the many cases with $M_{\text{KK}} = 2 \text{ TeV}$. By contraries, in all the low cutoff cases in Figs. 8,9,10, the threshold correction plays a very important role. Here we mention that the cases with $m_h = 145 \text{ GeV}$ are almost identical with these with $m_h = 120 \text{ GeV}$.
- In the Higgs decay to two photons in each model, unlike with the previous gluon fusion case, the interference term between the threshold correction and the UED effect is constructive (destructive) in case of $C_{h\gamma\gamma} = +1$ (-1), respectively. In this case, the degree of the effect which only comes from the threshold correction is also smaller than the others. It is an interesting point that in some cases with $C_{g\gamma\gamma} = +1$, the value of the ratio ($\mathcal{R}_{h^{(0)} \rightarrow 2\gamma}$) exceeds one, which we never find in the no-threshold-correction cases in the range of the parameter region of M_{KK} which we consider. Another remarkable point compared to the gluon fusion, the cases with $m_h = 145 \text{ GeV}$ are not identical with these with $m_h = 120 \text{ GeV}$ but this difference is still not so significant since the other effects (cutoff scale, threshold correction and so on) are more effective. Of course, in all the low cutoff cases in Figs. 11,12,13, the threshold correction works very well. We mention that we can find the $10 \sim 20\%$ deviations from the no-threshold-correction cases even with $M_{\text{KK}} = 2 \text{ TeV}$ in all the 6D UED models.
- After combining the above two results, we can estimate the total ratio Δ in each 6D UED model with the extremal threshold corrections. In this analysis, we only consider the $m_h = 120 \text{ GeV}$ cases. There are nine curves in each graph and our convention about the color/shape of curves is summarized in Table 5. Here we would like to only focus on a few important topics. Firstly, we can find the tendency that every orange line ($C_{hgg} = -1, C_{h\gamma\gamma} = +1$) is located at the top of each graph and any cyan one ($C_{hgg} = +1, C_{h\gamma\gamma} = -1$) is located at the bottom of each graph. The reason is that the two threshold corrections function toward maximally enhancing (suppressing) the process in the former (latter) case. Secondly, the deviation from the no-threshold-correction case (black dot-dashed curve) is noteworthy, in particular, in the M_{KK} range below 1 TeV . All the results tend to converge with the no-threshold-correction curve proportional to the value of M_{KK} and it is notable even around $M_{\text{KK}} = 2 \text{ TeV}$ in many choices of C_{hgg} and $C_{h\gamma\gamma}$ because the tens of percents of the deviations still remain. Thirdly, in the low cutoff cases, the interference effects dominate the whole process and the predictions about two photon signals via the gluon fusion Higgs production possibly become extraordinary. Finally we comment on the constraint

from the LHC results briefly. We also do not execute detailed analysis in this case but we can conclude that some cases which predict too great value of the total ratio are already excluded. On the other hand, the total ratio can be suppressed in some choices of the parameters describing the threshold corrections, and in this case the possibility with $m_h = 145$ GeV is not totally rejected.

At the end of this section, we give comments for more precise analysis. We need to take into account the correction from QCD (parton distribution function and K-factor) [83]. However the KK contributions would receive almost the same QCD corrections as in the case of the SM and this deviation from the SM result would not be large. Actually, to get the ratios of event rates in 6D UED models to that in the SM, the partial decay width in Δ should be replaced by corresponding branching ratios. We, however, expect that the effects of heavy KK particles to the leading decay processes at the tree level are small because of decoupling. Thus Δ is expected to be enough for crude estimation. But there are two other one-loop leading decay processes of $h^{(0)} \rightarrow 2g$ and $h^{(0)} \rightarrow \gamma Z$, which may possibly give considerable contribution to the Branching Ratio. These points are beyond the scope of this paper and are left for future work [84].

7 Summary

In this paper, we have discussed the main Higgs production process through gluon fusion and the important one-loop leading decay channel to two photons at the LHC in various 6D UED models. The Higgs production cross sections in 6D UED models are much enhanced than the prediction of the SM or the 5D mUED. In contrast, the decay width in 6D UED models are decreased because of the destructive contribution between quarks and gauge bosons. In both cases, the results of *PS* model are significant. This is because numerous fermions contribute to the process in each level of KK modes. We also have discussed the threshold corrections in the processes and their effects become significant even when we take the higher cutoff and/or a heavy KK scale. Some parameter region are already excluded by the current LHC experimental results obviously. By use of the data announced by the ATLAS and CMS experiments in the December of 2011, we can estimate the lower bounds of the KK scale as $M_{\text{KK}} = 600 (T^2/Z_4)$, $750 (S^2/Z_2)$, $1150 (PS)$ GeV when we consider the high cutoffs with no threshold correction. These results are modified by the threshold corrections substantially. The SM with the 145 GeV Higgs boson is rejected but 6D UED with the Higgs mass parameter is still survived in some ranges of the parameters describing the threshold corrections.

Our results are affected by ultraviolet physics because the calculation has logarithmic cutoff scale dependence. There seem to be some ambiguities coming from this fact. We expect that our prediction would be verified by forthcoming LHC experimental results. Detailed analysis of the final states in the single Higgs production at the LHC is important for discriminating UED from the other models.

The collider physics and particle cosmology of S^2 -based 6D UED models are unexplored and we would like to pursue these topics in future work [76, 84].

Acknowledgments

We are most grateful to C. S. Lim and Kin-ya Oda for valuable comments and discussions. In particular C. S. Lim read the manuscript carefully and gave us very useful comments. And we also thank Nobuhito Maru, Naoya Okuda, Makoto Sakamoto, Joe Sato, Takashi Shimomura, Ryoutaro Watanabe and Masato Yamanaka for fruitful discussions. Yasuhiro Okada and Hideo Ito suggest the recent Tevatron experimental results to us. We express our appreciation to them very much. We again appreciate C. S. Lim and Kin-ya Oda for advising me in the revision. Finally we appreciate the referee for giving a lot of useful comments.

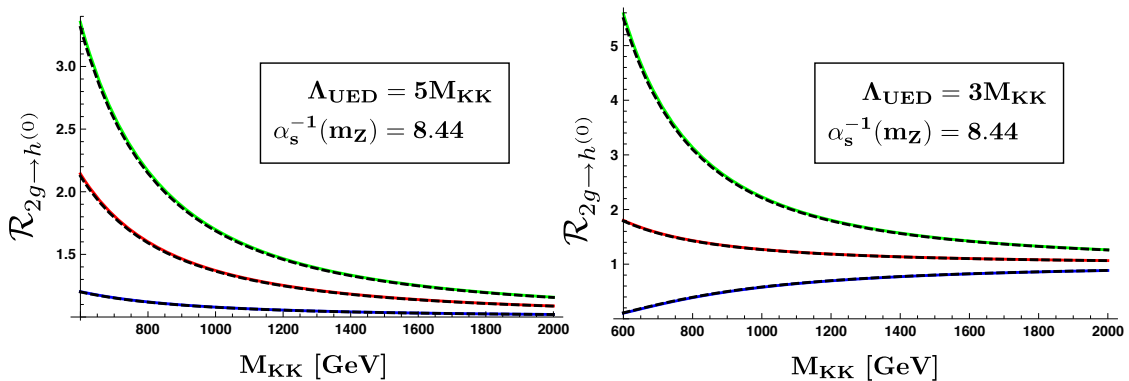


Figure 8. These plots represent the values of the ratios $\mathcal{R}_{2g \rightarrow h^{(0)}}$ in 6D UED on T^2/Z_4 with/without threshold correction. The red, blue, green curves show these with $C_{hgg} = 0, +1, -1$, respectively. Each black dashed line near the lines for $m_h = 120$ GeV corresponds to that with $m_h = 145$ GeV. In the left and right plots, which correspond to the high and low cutoff cases, respectively, we take the value of the QCD coupling strength as that at the Z boson mass scale.

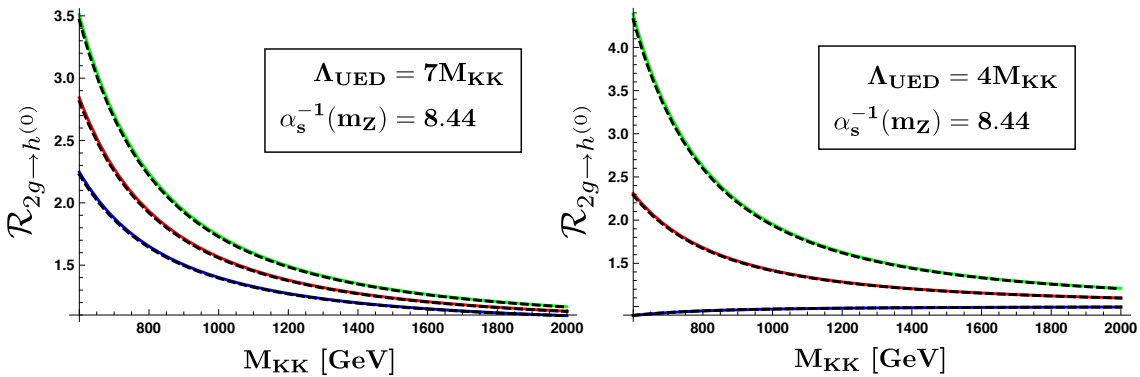


Figure 9. These plots represent the values of the ratios $\mathcal{R}_{2g \rightarrow h^{(0)}}$ in 6D UED on S^2/Z_2 with/without threshold correction. The red, blue, green curves show these with $C_{hgg} = 0, +1, -1$, respectively. Each black dashed line near the lines for $m_h = 120$ GeV corresponds to that with $m_h = 145$ GeV. In the left and right plots, which correspond to the high and low cutoff cases, respectively, we take the value of the QCD coupling strength as that at the Z boson mass scale.

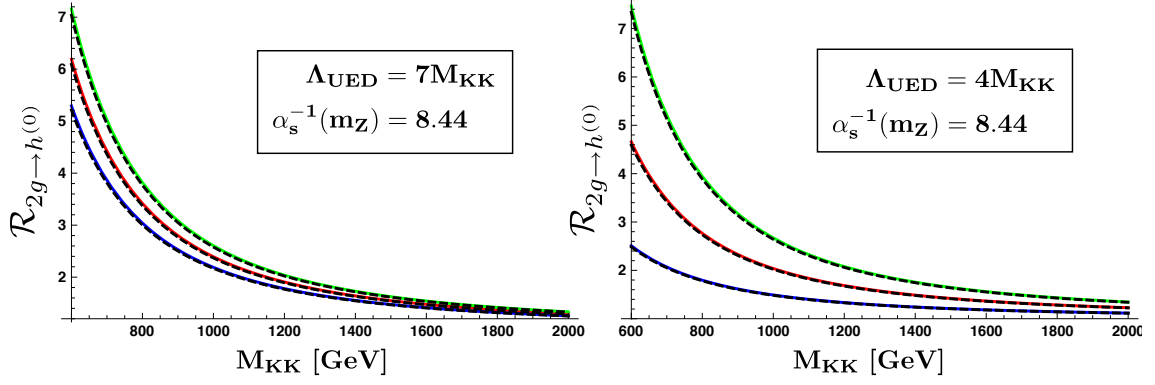


Figure 10. These plots represent the values of the ratios $\mathcal{R}_{2g \rightarrow h^{(0)}}$ in 6D UED on PS with/without threshold correction. The red, blue, green curves show these with $C_{hgg} = 0, +1, -1$, respectively. Each black dashed line near the lines for $m_h = 120$ GeV corresponds to that with $m_h = 145$ GeV. In the left and right plots, which correspond to the high and low cutoff cases, respectively, we take the value of the QCD coupling strength as that at the Z boson mass scale.

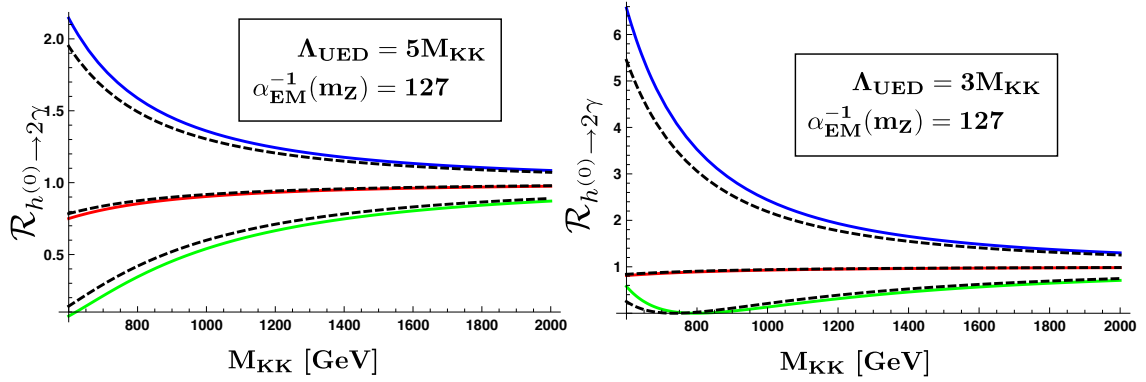


Figure 11. These plots represent the values of the ratios $\mathcal{R}_{h^{(0)} \rightarrow 2\gamma}$ in 6D UED on T^2/Z_4 with/without threshold correction. The red, blue, green curves show these with $C_{h\gamma\gamma} = 0, +1, -1$, respectively. Each black dashed line near the lines for $m_h = 120$ GeV corresponds to that with $m_h = 145$ GeV. In the left and right plots, which correspond to the high and low cutoff cases, respectively, we take the value of the electromagnetic coupling strength as that at the Z boson mass scale.

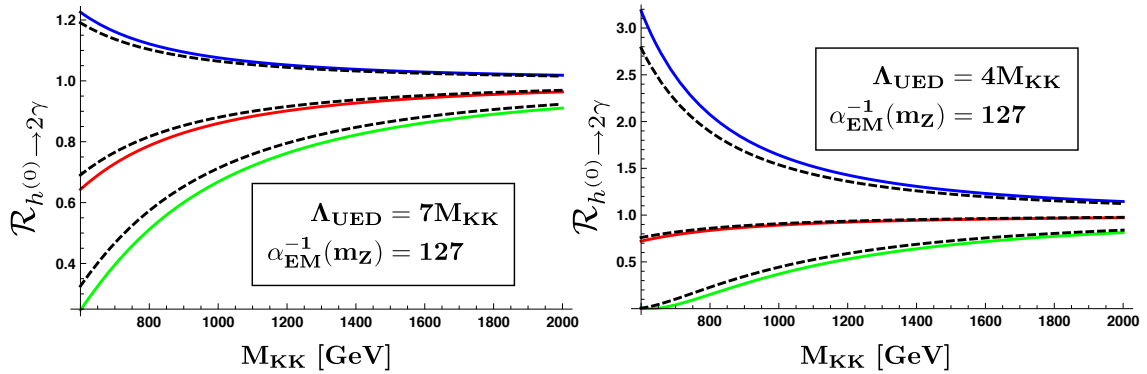


Figure 12. These plots represent the values of the ratios $\mathcal{R}_{h^{(0)} \rightarrow 2\gamma}$ in 6D UED on S^2/Z_2 with/without threshold correction. The red, blue, green curves show these with $C_{h\gamma\gamma} = 0, +1, -1$, respectively. Each black dashed line near the lines for $m_h = 120$ GeV corresponds to that with $m_h = 145$ GeV. In the left and right plots, which correspond to the high and low cutoff cases, respectively, we take the value of the electromagnetic coupling strength as that at the Z boson mass scale.

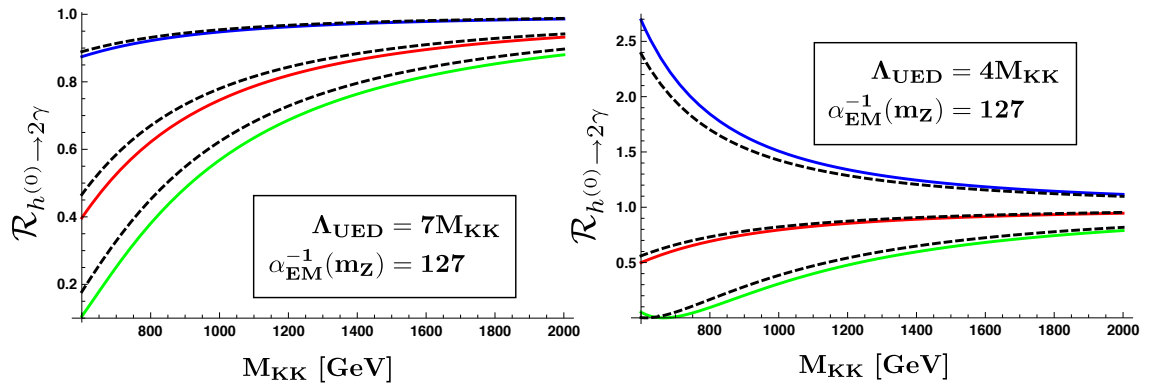


Figure 13. These plots represent the values of the ratios $\mathcal{R}_{h^{(0)} \rightarrow 2\gamma}$ in 6D UED on PS with/without threshold correction. The red, blue, green curves show these with $C_{h\gamma\gamma} = 0, +1, -1$, respectively. Each black dashed line near the lines for $m_h = 120$ GeV corresponds to that with $m_h = 145$ GeV. In the left and right plots, which correspond to the high and low cutoff cases, respectively, we take the value of the electromagnetic coupling strength as that at the Z boson mass scale.

value of C_{hgg}	value of $C_{h\gamma\gamma}$	color/shape of curve
$C_{hgg} = 0$	$C_{h\gamma\gamma} = 0$	black, dot-dashed
$C_{hgg} = +1$	$C_{h\gamma\gamma} = 0$	red
$C_{hgg} = 0$	$C_{h\gamma\gamma} = +1$	blue
$C_{hgg} = -1$	$C_{h\gamma\gamma} = 0$	green
$C_{hgg} = 0$	$C_{h\gamma\gamma} = -1$	magenta
$C_{hgg} = +1$	$C_{h\gamma\gamma} = +1$	yellow, dotted
$C_{hgg} = -1$	$C_{h\gamma\gamma} = +1$	orange, dotted
$C_{hgg} = +1$	$C_{h\gamma\gamma} = -1$	cyan, dotted
$C_{hgg} = -1$	$C_{h\gamma\gamma} = -1$	brown, dotted

Table 5. Our convention about the color/shape of curves in Figs. 14,15,16 (total ratios).

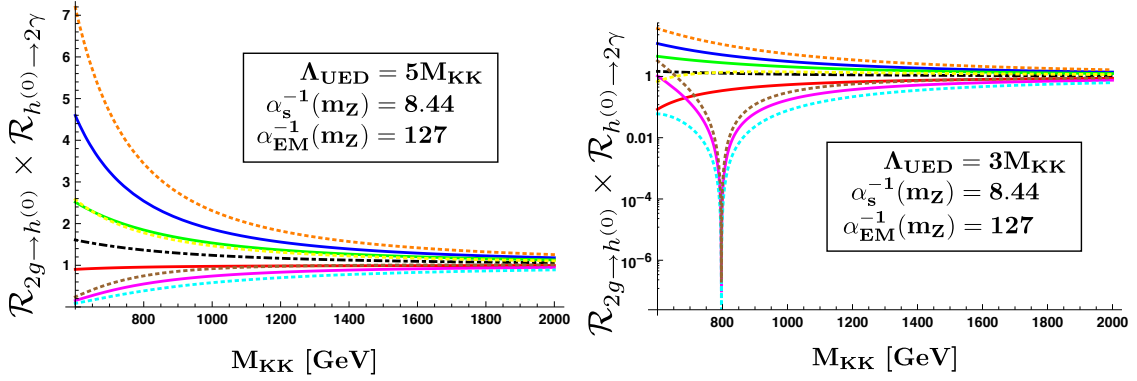


Figure 14. These plots represent the values of the total ratios Δ in 6D UED on T^2/Z_4 with/without threshold corrections with $m_h = 120$ GeV. The color/shape convention is summarized in Table 5. In the left and right plots, which correspond to the high and low cutoff cases, respectively, we take the values of the QCD and electromagnetic coupling strengths as that at the Z boson mass scale.

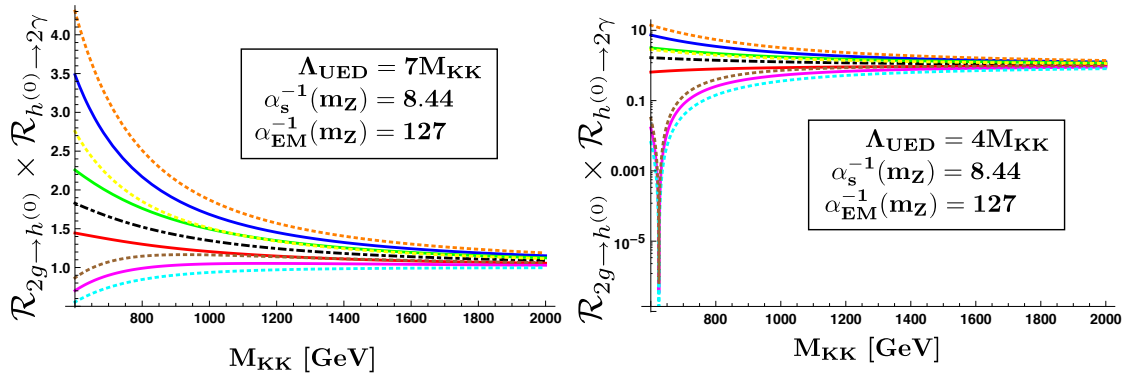


Figure 15. These plots represent the values of the total ratios Δ in 6D UED on S^2/Z_2 with/without threshold corrections with $m_h = 120$ GeV. The color/shape convention is summarized in Table 5. In the left and right plots, which correspond to the high and low cutoff cases, respectively, we take the values of the QCD and electromagnetic coupling strengths as that at the Z boson mass scale.

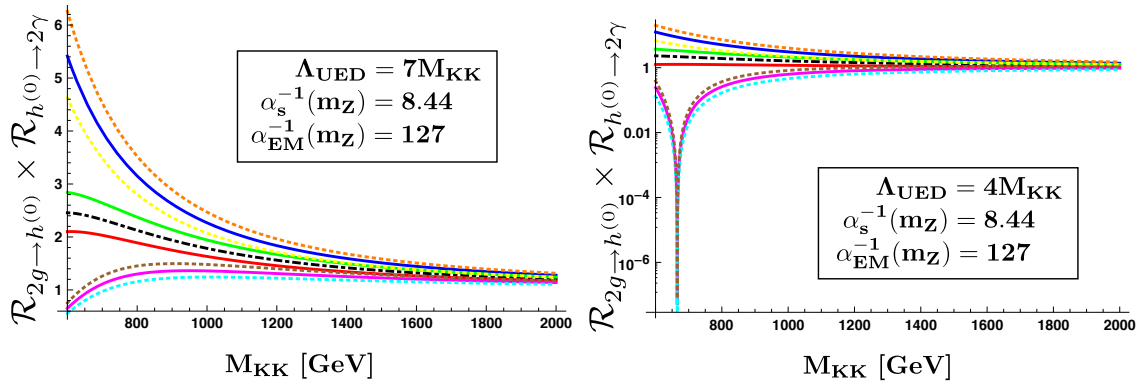


Figure 16. These plots represent the values of the total ratios Δ in 6D UED on PS with/without threshold corrections with $m_h = 120$ GeV. The color/shape convention is summarized in Table 5. In the left and right plots, which correspond to the high and low cutoff cases, respectively, we take the values of the QCD and electromagnetic coupling strengths as that at the Z boson mass scale.

A Feynman Rules containing scalar particle

In this appendix, we list the Feynman rules containing scalar particle in the 't Hooft-Feynman gauge. We omit the rules containing no scalar particle, which are the same with the corresponding rules of the SM for the zero modes alone. In the vertices all momenta (k_1, k_2) and directions of propagation are considered as incoming. $g^{(2)}$ and e are $SU(2)_L$ the 4D gauge coupling and the 4D elementary electric charge, respectively.

$$= -i(k_1 - k_2)_\mu \mathcal{F},$$

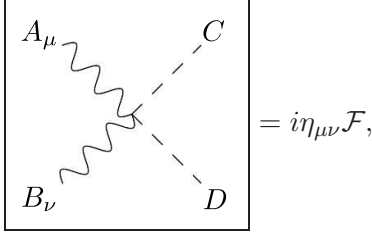
A_μ	B	C	\mathcal{F}
$W_\mu^+(m,n)$	$G^-(m,n)$	$h(0)$	$\frac{g^{(2)}}{2} \frac{-im_W}{m_{W,(m,n)}}$
$W_\mu^+(m,n)$	$a^-(m,n)$	$h(0)$	$\frac{g^{(2)}}{2} \frac{m(m,n)}{m_{W,(m,n)}}$
$W_\mu^-(m,n)$	$G^+(m,n)$	$h(0)$	$\frac{g^{(2)}}{2} \frac{-im_W}{m_{W,(m,n)}}$
$W_\mu^-(m,n)$	$a^+(m,n)$	$h(0)$	$\frac{g^{(2)}}{2} \frac{-m(m,n)}{m_{W,(m,n)}}$
$A_\mu^{(0)}$	$G^+(m,n)$	$G^-(m,n)$	e
$A_\mu^{(0)}$	$a^+(m,n)$	$a^-(m,n)$	e
$A_\mu^{(0)}$	$H^+(m,n)$	$H^-(m,n)$	e

$$= i\eta_{\mu\nu} \mathcal{F},$$

A	B_μ	C_ν	\mathcal{F}
$h(0)$	$W_\mu^+(m,n)$	$W_\nu^-(m,n)$	$m_W g^{(2)}$
$G^+(m,n)$	$W_\mu^-(m,n)$	$A_\nu^{(0)}$	$-iem_{W,(m,n)}$
$G^-(m,n)$	$W_\mu^+(m,n)$	$A_\nu^{(0)}$	$iem_{W,(m,n)}$

$$= -im_W g^{(2)} \mathcal{F},$$

A	B	C	\mathcal{F}
$h(0)$	$G^+(m,n)$	$G^-(m,n)$	$\frac{m_h^2}{2m_{W,(m,n)}^2}$
$h(0)$	$G^+(m,n)$	$a^-(m,n)$	$i \frac{m(m,n)}{2m_{W,(m,n)}^2} \left(\frac{m_h^2}{m_W} - \frac{m_{W,(m,n)}^2}{m_W} \right)$
$h(0)$	$a^+(m,n)$	$G^-(m,n)$	$i \frac{m(m,n)}{2m_{W,(m,n)}^2} \left(-\frac{m_h^2}{m_W} + \frac{m_{W,(m,n)}^2}{m_W} \right)$
$h(0)$	$a^+(m,n)$	$a^-(m,n)$	$\frac{1}{2m_{W,(m,n)}^2} \left(\frac{m_h^2}{m_W^2} m(m,n)^2 + 2m_{W,(m,n)}^2 \right)$
$h(0)$	$H^+(m,n)$	$H^-(m,n)$	1



A_μ	B_ν	C	D	\mathcal{F}
$W_\mu^{+(m,n)}$	$A_\nu^{(0)}$	$G^{-(m,n)}$	$h^{(0)}$	$\frac{eg^{(2)}}{2} \left(\frac{-im_W}{m_{W,(m,n)}} \right)$
$W_\mu^{-(m,n)}$	$A_\nu^{(0)}$	$G^{+(m,n)}$	$h^{(0)}$	$\frac{eg^{(2)}}{2} \left(\frac{-im_W}{m_{W,(m,n)}} \right)$
$W_\mu^{+(m,n)}$	$A_\nu^{(0)}$	$a^{-(m,n)}$	$h^{(0)}$	$\frac{eg^{(2)}}{2} \left(\frac{-m_{(m,n)}}{m_{W,(m,n)}} \right)$
$W_\mu^{-(m,n)}$	$A_\nu^{(0)}$	$a^{+(m,n)}$	$h^{(0)}$	$\frac{eg^{(2)}}{2} \left(\frac{-m_{(m,n)}}{m_{W,(m,n)}} \right)$
$A_\mu^{(0)}$	$A_\nu^{(0)}$	$G^{+(m,n)}$	$G^{-(m,n)}$	$2e^2$
$A_\mu^{(0)}$	$A_\nu^{(0)}$	$a^{+(m,n)}$	$a^{-(m,n)}$	$2e^2$
$A_\mu^{(0)}$	$A_\nu^{(0)}$	$H^{+(m,n)}$	$H^{-(m,n)}$	$2e^2$

B Detail on threshold correction

In this Appendix, we explain the concrete forms of threshold corrections in the gluon fusion ($2g \rightarrow h^{(0)}$) and the Higgs decay to two photons ($h^{(0)} \rightarrow 2\gamma$). The parts of the Lagrangian describing the former (\mathcal{L}_{hgg}) and the latter ($\mathcal{L}_{h\gamma\gamma}$) processes are defined as

$$\mathcal{L}_{hgg} = -\frac{1}{4} \frac{C_{hgg}}{\Lambda_{\text{UED}}^2} V_2 F_{MN}^{[\text{QCD}]} F^{[\text{QCD}]}{}^{MN} H^\dagger H, \quad (\text{B.1})$$

$$\mathcal{L}_{h\gamma\gamma} = -\frac{1}{4} \frac{C_{h\gamma\gamma}}{\Lambda_{\text{UED}}^2} V_2 F_{MN}^{[\text{QED}]} F^{[\text{QED}]}{}^{MN} H^\dagger H, \quad (\text{B.2})$$

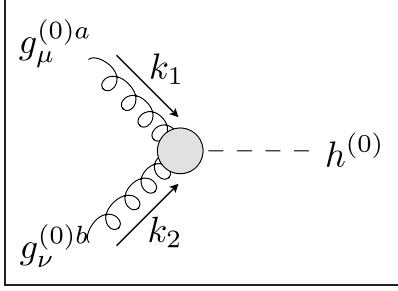
where C_{hgg} and $C_{h\gamma\gamma}$ are dimensionless coefficients characterizing the processes, Λ_{UED} is 6D UED cutoff, V_2 is the volume of the two extra dimensions, H is the 6D Higgs doublet, and $F_{MN}^{[\text{QCD}]}$ ($F_{MN}^{[\text{QED}]}$) is the 6D field strength of gluon (photon), respectively. It is an important thing that the Higgs doublet should be introduced in these effective operators in a bilinear form of $H^\dagger H$ because the electroweak symmetry breaking (EWSB) is realized by the usual Higgs mechanism in 6D UED models. After EWSB and KK reduction, the Higgs doublet can acquire the VEV as $\langle H \rangle = (0, v)^T / \sqrt{2V_2}$, where $v \simeq 246 \text{ GeV}$, and we would like to focus on the parts, which are

$$\mathcal{L}_{hgg} \supset -\frac{v/\sqrt{2}}{4} \frac{C_{hgg}}{\Lambda_{\text{UED}}^2} F_{\mu\nu}^{(0)[\text{QCD}]} F^{(0)[\text{QCD}]}{}_{\mu\nu} h^{(0)}, \quad (\text{B.3})$$

$$\mathcal{L}_{h\gamma\gamma} \supset -\frac{v/\sqrt{2}}{4} \frac{C_{h\gamma\gamma}}{\Lambda_{\text{UED}}^2} F_{\mu\nu}^{(0)[\text{QED}]} F^{(0)[\text{QED}]}{}_{\mu\nu} h^{(0)}. \quad (\text{B.4})$$

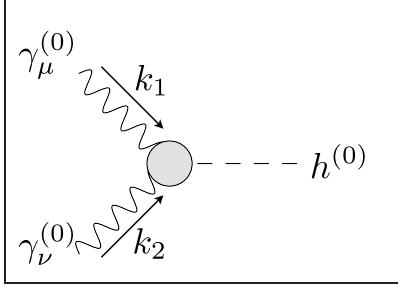
The superscript “(0)” means that the fields are zero modes and we take integration toward the two extra spacial directions in Eqs. (B.3) and (B.4). The two operators are understood as dimension-six operators in 4D point of view. Finally, we write down the concrete forms

of Feynman rules as follows:



The diagram shows a central grey circle representing a vertex. Two incoming gluon lines, represented by curly arrows, enter from the left. The top-left line is labeled $g_\mu^{(0)a}$ and has momentum k_1 . The bottom-left line is labeled $g_\nu^{(0)b}$ and has momentum k_2 . A dashed line representing a Higgs boson $h^{(0)}$ exits to the right.

$$= -i \frac{C_{hgg} v / \sqrt{2}}{\Lambda_{\text{UED}}^2} (k_{2\mu} k_{1\nu} - (k_1 \cdot k_2) \eta_{\mu\nu}) \delta^{ab}, \quad (\text{B.5})$$



The diagram shows a central grey circle representing a vertex. Two incoming photon lines, represented by wavy arrows, enter from the left. The top-left line is labeled $\gamma_\mu^{(0)}$ and has momentum k_1 . The bottom-left line is labeled $\gamma_\nu^{(0)}$ and has momentum k_2 . A dashed line representing a Higgs boson $h^{(0)}$ exits to the right.

$$= -i \frac{C_{h\gamma\gamma} v / \sqrt{2}}{\Lambda_{\text{UED}}^2} (k_{2\mu} k_{1\nu} - (k_1 \cdot k_2) \eta_{\mu\nu}), \quad (\text{B.6})$$

where a, b are gluon indices.

References

- [1] N. Arkani-Hamed, S. Dimopoulos, and G. R. Dvali, *The hierarchy problem and new dimensions at a millimeter*, *Phys. Lett.* **B429** (1998) 263–272, [[hep-ph/9803315](#)].
- [2] L. Randall and R. Sundrum, *A large mass hierarchy from a small extra dimension*, *Phys. Rev. Lett.* **83** (1999) 3370–3373, [[hep-ph/9905221](#)].
- [3] I. Antoniadis, *A Possible new dimension at a few TeV*, *Phys. Lett.* **B246** (1990) 377–384.
- [4] T. Appelquist, H.-C. Cheng, and B. A. Dobrescu, *Bounds on universal extra dimensions*, *Phys. Rev.* **D64** (2001) 035002, [[hep-ph/0012100](#)].
- [5] K. Agashe, N. G. Deshpande, and G. H. Wu, *Can extra dimensions accessible to the SM explain the recent measurement of anomalous magnetic moment of the muon?*, *Phys. Lett.* **B511** (2001) 85–91, [[hep-ph/0103235](#)].
- [6] K. Agashe, N. G. Deshpande, and G. H. Wu, *Universal extra dimensions and $b \rightarrow s$ gamma*, *Phys. Lett.* **B514** (2001) 309–314, [[hep-ph/0105084](#)].
- [7] T. Appelquist and B. A. Dobrescu, *Universal extra dimensions and the muon magnetic moment*, *Phys. Lett.* **B516** (2001) 85–91, [[hep-ph/0106140](#)].
- [8] T. Appelquist and H.-U. Yee, *Universal extra dimensions and the Higgs boson mass*, *Phys. Rev.* **D67** (2003) 055002, [[hep-ph/0211023](#)].
- [9] J. F. Oliver, J. Papavassiliou, and A. Santamaria, *Universal extra dimensions and $Z \rightarrow b$ anti- b* , *Phys. Rev.* **D67** (2003) 056002, [[hep-ph/0212391](#)].
- [10] D. Chakraverty, K. Huitu, and A. Kundu, *Effects of Universal Extra Dimensions on $B^0 - \bar{B}^0$ Mixing*, *Phys. Lett.* **B558** (2003) 173–181, [[hep-ph/0212047](#)].

- [11] A. J. Buras, M. Spranger, and A. Weiler, *The Impact of Universal Extra Dimensions on the Unitarity Triangle and Rare K and B Decays*, *Nucl. Phys.* **B660** (2003) 225–268, [[hep-ph/0212143](#)].
- [12] P. Colangelo, F. De Fazio, R. Ferrandes, and T. N. Pham, *Exclusive $B \rightarrow K^{(*)}l_+l_-$, $B \rightarrow K^{(*)}\nu\bar{\nu}$ and $B \rightarrow K^*\gamma$ transitions in a scenario with a single universal extra dimension*, *Phys. Rev.* **D73** (2006) 115006, [[hep-ph/0604029](#)].
- [13] I. Gogoladze and C. Macesanu, *Precision electroweak constraints on Universal Extra Dimensions revisited*, *Phys. Rev.* **D74** (2006) 093012, [[hep-ph/0605207](#)].
- [14] H.-C. Cheng, J. L. Feng, and K. T. Matchev, *Kaluza-Klein dark matter*, *Phys. Rev. Lett.* **89** (2002) 211301, [[hep-ph/0207125](#)].
- [15] G. Servant and T. M. P. Tait, *Is the lightest Kaluza-Klein particle a viable dark matter candidate?*, *Nucl. Phys.* **B650** (2003) 391–419, [[hep-ph/0206071](#)].
- [16] M. Kakizaki, S. Matsumoto, Y. Sato, and M. Senami, *Significant effects of second KK particles on LKP dark matter physics*, *Phys. Rev.* **D71** (2005) 123522, [[hep-ph/0502059](#)].
- [17] S. Matsumoto and M. Senami, *Efficient coannihilation process through strong Higgs self-coupling in LKP dark matter annihilation*, *Phys. Lett.* **B633** (2006) 671–674, [[hep-ph/0512003](#)].
- [18] F. Burnell and G. D. Kribs, *The abundance of Kaluza-Klein dark matter with coannihilation*, *Phys. Rev.* **D73** (2006) 015001, [[hep-ph/0509118](#)].
- [19] M. Kakizaki, S. Matsumoto, and M. Senami, *Relic abundance of dark matter in the minimal universal extra dimension model*, *Phys. Rev.* **D74** (2006) 023504, [[hep-ph/0605280](#)].
- [20] K. Kong and K. T. Matchev, *Precise calculation of the relic density of Kaluza-Klein dark matter in universal extra dimensions*, *JHEP* **01** (2006) 038, [[hep-ph/0509119](#)].
- [21] S. Matsumoto, J. Sato, M. Senami, and M. Yamanaka, *Relic abundance of dark matter in universal extra dimension models with right-handed neutrinos*, *Phys. Rev.* **D76** (2007) 043528, [[arXiv:0705.0934](#)].
- [22] M. Kakizaki, S. Matsumoto, Y. Sato, and M. Senami, *Relic abundance of LKP dark matter in UED model including effects of second KK resonances*, *Nucl. Phys.* **B735** (2006) 84–95, [[hep-ph/0508283](#)].
- [23] G. Belanger, M. Kakizaki, and A. Pukhov, *Dark matter in UED: The Role of the second KK level*, *JCAP* **1102** (2011) 009, [[arXiv:1012.2577](#)].
- [24] J. Hisano, K. Ishiwata, N. Nagata, and M. Yamanaka, *Direct Detection of Vector Dark Matter*, *Prog.Theor.Phys.* **126** (2011) 435–456, [[arXiv:1012.5455](#)].
- [25] H.-C. Cheng, K. T. Matchev, and M. Schmaltz, *Bosonic supersymmetry? Getting fooled at the CERN LHC*, *Phys. Rev.* **D66** (2002) 056006, [[hep-ph/0205314](#)].
- [26] A. Datta, K. Kong, and K. T. Matchev, *Discrimination of supersymmetry and universal extra dimensions at hadron colliders*, *Phys. Rev.* **D72** (2005) 096006, [[hep-ph/0509246](#)].
- [27] S. Matsumoto, J. Sato, M. Senami, and M. Yamanaka, *Productions of second Kaluza-Klein gauge bosons in the minimal universal extra dimension model at LHC*, *Phys. Rev.* **D80** (2009) 056006, [[arXiv:0903.3255](#)].
- [28] B. A. Dobrescu and E. Poppitz, *Number of fermion generations derived from anomaly cancellation*, *Phys. Rev. Lett.* **87** (2001) 031801, [[hep-ph/0102010](#)].

- [29] T. Appelquist, B. A. Dobrescu, E. Ponton, and H.-U. Yee, *Proton stability in six dimensions*, *Phys. Rev. Lett.* **87** (2001) 181802, [[hep-ph/0107056](#)].
- [30] N. Arkani-Hamed, H.-C. Cheng, B. A. Dobrescu, and L. J. Hall, *Self-breaking of the standard model gauge symmetry*, *Phys. Rev.* **D62** (2000) 096006, [[hep-ph/0006238](#)].
- [31] M. Hashimoto, M. Tanabashi, and K. Yamawaki, *Topped MAC with extra dimensions?*, *Phys. Rev.* **D69** (2004) 076004, [[hep-ph/0311165](#)].
- [32] M. Hashimoto and D. K. Hong, *Topcolor breaking through boundary conditions*, *Phys. Rev.* **D71** (2005) 056004, [[hep-ph/0409223](#)].
- [33] H.-C. Cheng, K. T. Matchev, and M. Schmaltz, *Radiative corrections to Kaluza-Klein masses*, *Phys. Rev.* **D66** (2002) 036005, [[hep-ph/0204342](#)].
- [34] E. Ponton and L. Wang, *Radiative effects on the chiral square*, *JHEP* **11** (2006) 018, [[hep-ph/0512304](#)].
- [35] G. Burdman, B. A. Dobrescu, and E. Ponton, *Resonances from two universal extra dimensions*, *Phys. Rev.* **D74** (2006) 075008, [[hep-ph/0601186](#)].
- [36] B. A. Dobrescu, K. Kong, and R. Mahbubani, *Leptons and photons at the LHC: Cascades through spinless adjoints*, *JHEP* **07** (2007) 006, [[hep-ph/0703231](#)].
- [37] B. A. Dobrescu, D. Hooper, K. Kong, and R. Mahbubani, *Spinless photon dark matter from two universal extra dimensions*, *JCAP* **0710** (2007) 012, [[arXiv:0706.3409](#)].
- [38] A. Freitas and K. Kong, *Two universal extra dimensions and spinless photons at the ILC*, *JHEP* **02** (2008) 068, [[arXiv:0711.4124](#)].
- [39] A. Freitas and U. Haisch, *Anti- $B \rightarrow X(s)$ gamma in two universal extra dimensions*, *Phys. Rev.* **D77** (2008) 093008, [[arXiv:0801.4346](#)].
- [40] K. Ghosh and A. Datta, *Probing two Universal Extra Dimensions at International Linear Collider*, *Phys. Lett.* **B665** (2008) 369–373, [[arXiv:0802.2162](#)].
- [41] G. Bertone, C. B. Jackson, G. Shaughnessy, T. M. P. Tait, and A. Vallinotto, *The WIMP Forest: Indirect Detection of a Chiral Square*, *Phys. Rev.* **D80** (2009) 023512, [[arXiv:0904.1442](#)].
- [42] M. Blennow, H. Melbeus, and T. Ohlsson, *Neutrinos from Kaluza-Klein dark matter in the Sun*, *JCAP* **1001** (2010) 018, [[arXiv:0910.1588](#)].
- [43] B. A. Dobrescu and E. Ponton, *Chiral compactification on a square*, *JHEP* **03** (2004) 071, [[hep-th/0401032](#)].
- [44] G. Burdman, B. A. Dobrescu, and E. Ponton, *Six-dimensional gauge theory on the chiral square*, *JHEP* **02** (2006) 033, [[hep-ph/0506334](#)].
- [45] G. Cacciapaglia, A. Deandrea, and J. Llodra-Perez, *A Dark Matter candidate from Lorentz Invariance in 6 Dimensions*, *JHEP* **03** (2010) 083, [[arXiv:0907.4993](#)].
- [46] N. Maru, T. Nomura, J. Sato, and M. Yamanaka, *The Universal Extra Dimensional Model with S^2/Z_2 extra-space*, *Nucl. Phys.* **B830** (2010) 414–433, [[arXiv:0904.1909](#)].
- [47] H. Dohi and K.-y. Oda, *Universal Extra Dimensions on Real Projective Plane*, *Phys. Lett.* **B692** (2010) 114–120, [[arXiv:1004.3722](#)].
- [48] T. Flacke, A. Menon, and D. J. Phalen, *Non-minimal universal extra dimensions*, *Phys. Rev.* **D79** (2009) 056009, [[arXiv:0811.1598](#)].

- [49] S. C. Park and J. Shu, *Split-UED and Dark Matter*, *Phys. Rev.* **D79** (2009) 091702, [[arXiv:0901.0720](#)].
- [50] C. Csaki, J. Heinonen, J. Hubisz, S. C. Park, and J. Shu, *5D UED: Flat and Flavorless*, *JHEP* **1101** (2011) 089, [[arXiv:1007.0025](#)].
- [51] N. Haba, K.-y. Oda, and R. Takahashi, *Top Yukawa Deviation in Extra Dimension*, *Nucl. Phys.* **B821** (2009) 74–128, [[arXiv:0904.3813](#)].
- [52] N. Haba, K.-y. Oda, and R. Takahashi, *Dirichlet Higgs in extra-dimension, consistent with electroweak data*, *Acta Phys.Polon.* **B42** (2011) 33–44, [[arXiv:0910.3356](#)].
- [53] N. Haba, K.-y. Oda, and R. Takahashi, *Diagonal Kaluza-Klein expansion under brane localized potential*, *Acta Phys. Polon.* **B41** (2010) 1291–1316, [[arXiv:0910.4528](#)].
- [54] N. Haba, K.-y. Oda, and R. Takahashi, *Phenomenological Aspects of Dirichlet Higgs Model from Extra-Dimension*, *JHEP* **07** (2010) 079, [[arXiv:1005.2306](#)].
- [55] K. Nishiwaki and K.-y. Oda, *Unitarity in Dirichlet Higgs Model*, *Eur.Phys.J.* **C71** (2011) 1786, [[arXiv:1011.0405](#)].
- [56] **The ATLAS collaboration** Collaboration, *Update of the Combination of Higgs Boson Searches in 1.0 to 2.3 fb⁻¹ of pp Collisions Data Taken at $\sqrt{s} = 7$ TeV with the ATLAS Experiment at the LHC*, . ATLAS NOTE, ATLAS-CONF-2011-135.
- [57] **The CMS collaboration** Collaboration, *Search for standard model Higgs boson in pp collisions at $\sqrt{s} = 7$ TeV and integrated luminosity up to 1.7 fb⁻¹*, . CMS PAS HIG-11-022.
- [58] **ATLAS Collaboration** Collaboration, G. Aad *et. al.*, *Combined search for the Standard Model Higgs boson using up to 4.9 fb⁻¹ of pp collision data at $\sqrt{s} = 7$ TeV with the ATLAS detector at the LHC*, *Phys.Lett.* **B710** (2012) 49–66, [[arXiv:1202.1408](#)].
- [59] **CMS Collaboration** Collaboration, S. Chatrchyan *et. al.*, *Combined results of searches for the standard model Higgs boson in pp collisions at $\sqrt{s} = 7$ TeV*, *Phys.Lett.* **B710** (2012) 26–48, [[arXiv:1202.1488](#)].
- [60] H. Georgi, A. K. Grant, and G. Hailu, *Brane couplings from bulk loops*, *Phys. Lett.* **B506** (2001) 207–214, [[hep-ph/0012379](#)].
- [61] C. S. Lim, N. Maru, and K. Nishiwaki, *CP Violation due to Compactification*, *Phys.Rev.* **D81** (2010) 076006, [[arXiv:0910.2314](#)].
- [62] C. A. Scrucca, M. Serone, L. Silvestrini, and A. Wulzer, *Gauge-Higgs Unification in Orbifold Models*, *JHEP* **02** (2004) 049, [[hep-th/0312267](#)].
- [63] H. M. Georgi, S. L. Glashow, M. E. Machacek, and D. V. Nanopoulos, *Higgs Bosons from Two Gluon Annihilation in Proton Proton Collisions*, *Phys. Rev. Lett.* **40** (1978) 692.
- [64] T. G. Rizzo, *GLUON FINAL STATES IN HIGGS BOSON DECAY*, *Phys. Rev.* **D22** (1980) 178.
- [65] F. J. Petriello, *Kaluza-Klein effects on Higgs physics in universal extra dimensions*, *JHEP* **05** (2002) 003, [[hep-ph/0204067](#)].
- [66] N. Maru, T. Nomura, J. Sato, and M. Yamanaka, *Higgs Production via Gluon Fusion in a Six Dimensional Universal Extra Dimension Model on S²/Z₂*, *Eur. Phys. J.* **C66** (2010) 283–287, [[arXiv:0905.4554](#)].
- [67] G. Passarino and M. J. G. Veltman, *One Loop Corrections for e+ e- Annihilation Into mu+*

- mu-* in the Weinberg Model, *Nucl. Phys.* **B160** (1979) 151.
- [68] A. Denner, *Techniques for calculation of electroweak radiative corrections at the one loop level and results for W physics at LEP-200*, *Fortschr. Phys.* **41** (1993) 307–420, [[arXiv:0709.1075](#)].
- [69] J. R. Ellis, M. K. Gaillard, and D. V. Nanopoulos, *A Phenomenological Profile of the Higgs Boson*, *Nucl. Phys.* **B106** (1976) 292.
- [70] S. Randjbar-Daemi, A. Salam, and J. A. Strathdee, *Spontaneous Compactification in Six-Dimensional Einstein-Maxwell Theory*, *Nucl. Phys.* **B214** (1983) 491–512.
- [71] E. T. Newman and R. Penrose, *Note on the Bondi-Metzner-Sachs group*, *J. Math. Phys.* **7** (1966) 863–870.
- [72] G. L. Smith *et. al.*, *Short range tests of the equivalence principle*, *Phys. Rev.* **D61** (2000) 022001.
- [73] C. A. Scrucca, M. Serone, and L. Silvestrini, *Electroweak symmetry breaking and fermion masses from extra dimensions*, *Nucl. Phys.* **B669** (2003) 128–158, [[hep-ph/0304220](#)].
- [74] K. R. Dienes, E. Dudas, and T. Gherghetta, *Extra spacetime dimensions and unification*, *Phys. Lett.* **B436** (1998) 55–65, [[hep-ph/9803466](#)].
- [75] K. R. Dienes, E. Dudas, and T. Gherghetta, *Grand unification at intermediate mass scales through extra dimensions*, *Nucl. Phys.* **B537** (1999) 47–108, [[hep-ph/9806292](#)].
- [76] K. Nishiwaki, K.-y. Oda, N. Okuda, and R. Watanabe, *Heavy Higgs at Tevatron and LHC in Universal Extra Dimension Models*, *Phys.Rev.* **D85** (2012) 035026, [[arXiv:1108.1765](#)].
- [77] T. Han, H. E. Logan, B. McElrath, and L.-T. Wang, *Loop induced decays of the little Higgs: $H \rightarrow g g$, $\gamma \gamma$* , *Phys. Lett.* **B563** (2003) 191–202, [[hep-ph/0302188](#)].
- [78] C. Dib, R. Rosenfeld, and A. Zerwekh, *Higgs production and decay in the little Higgs model*, [[hep-ph/0302068](#)].
- [79] C.-R. Chen, K. Tobe, and C. P. Yuan, *Higgs boson production and decay in little Higgs models with T-parity*, *Phys. Lett.* **B640** (2006) 263–271, [[hep-ph/0602211](#)].
- [80] A. Falkowski, *Pseudo-Goldstone Higgs Production via Gluon Fusion*, *Phys. Rev.* **D77** (2008) 055018, [[arXiv:0711.0828](#)].
- [81] N. Maru and N. Okada, *Gauge-Higgs Unification at LHC*, *Phys. Rev.* **D77** (2008) 055010, [[arXiv:0711.2589](#)].
- [82] N. Maru, *Finite Gluon Fusion Amplitude in the Gauge-Higgs Unification*, *Mod. Phys. Lett.* **A23** (2008) 2737–2750, [[arXiv:0803.0380](#)].
- [83] S. K. Rai, *UED effects on Higgs signals at LHC*, *Int. J. Mod. Phys.* **A23** (2008) 823–834, [[hep-ph/0510339](#)].
- [84] K. Nishiwaki, K.-y. Oda, N. Okuda, and R. Watanabe, *A Bound on Universal Extra Dimension Models from up to 2fb^{-1} of LHC Data at 7TeV* , *Phys.Lett.* **B707** (2012) 506–511, [[arXiv:1108.1764](#)].